**ANDRA BGR CRIEPI ENRESA GRS HSK IRSN JAEA
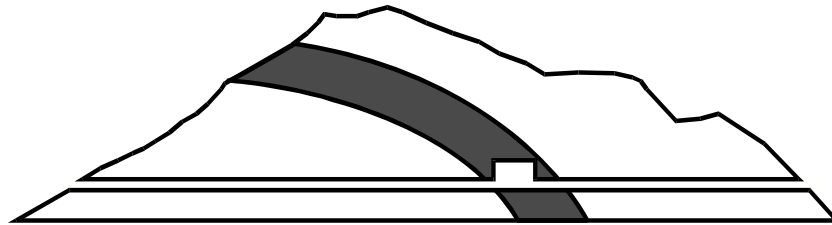NAGRA NWMO OBAYASHI SCK•CEN SWISSTOPO**

Mont Terri Project

TECHNICAL REPORT 2008-03
August 2008

Laboratory Testing of Opalinus Clay (LT) Experiment:
Comparison of Opalinus Clay and Callovo-Oxfordian clay-stone with respect to mechanical strength and carbonate microfabric

M. Klinkenberg, R. Dohrmann & S. Siegesmund

BGR, Germany

Distribution:

Standard distribution:

ANDRA (J. Delay)

BGR (H. J. Alheid)

CRIEPI (K. Kiho)

ENRESA (J. Astudillo)

GRS (T. Rothfuchs)

HSK (E. Frank)

IRSN (J.-M. Matray)

JAEA (N. Shigeta)

Nagra (M. Hugi)

NWMO (B. Belfadhel)

Obayashi (H. Kawamura, T. Tanaka)

SCK•CEN (G. Volckaert)

SWISSTOPO (P. Bossart and P. Hayoz)

GI AG (Ch. Nussbaum)

Additional distribution:

Every organisation & contractor takes care of their own distribution.

ABSTRACT

One important goal of clay science is to understand the relation of properties and performance of clays which is possible in limited cases, only. Obviously, the effect of certain properties of clays is not fully understood, yet. One of these properties is the arrangement of minerals within a clay (microfabric). In fact, the influence of clay microfabric on petrophysical properties is more often claimed than proved (Decher & Friedrich, 1991; Pusch et al., 1995; Bauer-Plaindoux et al., 1998; Pusch & Schomburg, 1999). The aim of this study was to find out, whether and to which degree, microfabric of clays can influence the petrophysical properties.

Clay-stones are currently being investigated as potential host rock for radioactive waste deposits. For this application hydraulic conductivity, swelling properties, water uptake, rheological, and mechanical properties are important. The most frequently studied clays are the Opalinus clay and the Callovo-Oxfordian clay-stone. One general goal is to establish a model for the prediction of mechanical behaviour of clays under repository-like conditions.

The carbonate content is known to significantly affect mechanical strength. However, Opalinus clay and Callovo-Oxfordian clay-stone behave different with respect to the dependence of mechanical strength on carbonate content. The failure strength of Opalinus clay decreases with increasing carbonate content while the failure strength of Callovo-Oxfordian clay-stone increases. This can be explained by the following observations: Opalinus clay contains large carbonate grains (mostly shell fragments) while Callovo-Oxfordium clay-stones contain fine-grained homogeneously distributed carbonates. The most important result of this work is that not only the carbonate content but also the grain size distribution, the shape and the distribution of carbonates determine the mechanical behaviour of the clay. In conclusion it is not possible to establish a mechanical model being applicable for clays in general. The present study proves that each type of clay has to be considered individually. Moreover, clay microfabric investigation may be a useful tool to understand the anisotropic behaviour of clay-stones.

TABLE OF CONTENTS

1   Introduction

Worldwide naturally occurring clay-stone formations are investigated with respect to the possibility of isolation of radioactive waste from the biosphere. Essential properties for the applicability of the geological barrier are impermeability towards aqueous solutions, mechanical strength, extensive thickness, and homogeneity (Nagra 1991, 2002). Clay-stones may be suitable for the sealing of waste material due to their specific properties (low hydraulic conductivity, swelling capacity, plasticity, pollutant retention). From geological history the enduring sealing properties of clay-stones are well known and are used in petroleum- and hydrogeology for exploration and protection of energy-resources (Eslinger & Pevear, 1988, Bjørlykke, 1989, Nagra, 1991, Lambert, 1997). Clay-stone formations occur near to the surface as well as in the deeper underground. For enduring and safe isolation of hazardous material deep formations are favoured. The "Arbeitskreis Auswahlverfahren Endlagerstandorte" (AkEnd) defined minimum standards for the host rock (AkEnd, 2002), which are fulfilled by clay-stone formations in Germany as well. These formations were presented by BGR (Hoth et al., 2007).

For the finalization of a repository, a performance assessment is necessary, which is based on models predicting the performance of the repository. For these models a substantial knowledge about the characteristics (physicochemical properties) of the rocks is necessary. The present study is focused on the question how mechanical properties of clay-stones depend on the mineralogical composition and the microfabric.

It is well known, that impermeability and mechanical strength depend on the structure on microscopic scale (1-100 µm = micro fabric). Changes of the microfabric influence the relevant extension and homogeneity of the geological barrier. The following properties of clay-stones, which also determine barrier characteristics, are significantly influenced by the microfabric (Aplin et al., 1999, Nagra, 2002):

- Porosity and permeability (Clennell et al., 1999, Pusch, 1999, Van Loon, 2002)
- Heat conductivity (Midtømme & Roaldstet, 1999)
- Plasticity
- Swelling properties (Decher & Friedrich, 1991)
- Mechanical strength (Petley, 1999)
- Retention and sorption (Sammartino et al., 2003, Yong, 2003, Yong & Mulligan, 2003)
- Stability against increased temperature and water vapour (Homm & Wehner, 2003)

In contrast, an influence of the clay-microfabric on the stability of the clay (minerals) against gamma-irradiation is not expected (Plötze et al., 2003).

The investigation of the clay microfabric is difficult due to the very fine grained material and its heterogeneity on different scales. In addition, the microfabric can be

changed by drying, rehydration, or oxidation, respectively. Until now, systematic studies about the influence of the fabric on the petrophysical properties like e.g. the mechanical behaviour of clay-stones are missing.

Clay-stones are a complex system consisting of different components e.g.: different (clay) minerals, rock (lithic) fragments, shell fragments, and porewater. Owing to the fine grain size, variable genesis, and texture these components are difficult to characterize. Furthermore, petrophysical/rock mechanical characteristics of clay-stones might change upon relatively small changes of the water content or other parameters (e.g. surrounding pressure).

This study is focused on Opalinus Clay, which is intensively investigated in the international URL Mont Terri, Switzerland (Nagra, 1991, 2002, Bossart & Thury, 2007). For comparison, the Callovo-Oxfordian Clay-stone of the URL Meuse/Haute-Marne in France (Delay et al., 2007) is considered.

The aim of this study is to find out if and how mechanical behaviour of clay-stones depends on microstructural characteristics. It is part of the Mont Terri experiment ‚Laboratory Testing (LT)', see Schnier & Stührenberg (2006).

1.1.   Clays and Clay minerals

Clay-stones are fine grained sedimentary clastic rocks, representing 65 % of all sediments and sedimentary rocks including low consolidated clays (Blatt, 1970, Stow & Piper, 1984).

There are numerous attempts to classify fine grained sediments and rocks (Ernst et al., 1959, Tourtelot, 1960, Pickard, 1971, Cole & Pickard, 1975, Lewan, 1979, Blatt et al., 1980, Potter et al., 1980, Stow & Piper, 1984, Füchtbauer, 1988, O'Brien & Slatt, 1990, Wignall, 1994, Macquacker & Adams, 2003). They are based on the following criteria.

•   Grain size (content of clay und silt fraction)

•   Composition (clay minerals, heavy minerals, organic material)

•   Fabric (existence and characteristic of bedding or cleavage).

According to DIN 4022 T1 the < 0.002 mm (< 2 µm) fraction of a soil or rock sample is defined as clay fraction.

A further classification of clay-stones is provided by Macquacker & Adams (2003; Fig. 1.1). This classification is predominantly descriptive and based on the grain size distribution (Fig. 1.1).

The AIPEA (Association Internationale pour l'Étude des Argiles) defines clay as: „…naturally occurring material composed primarily of fine-grained minerals, which is generally plastic at appropriate water contents and will harden with drying or firing. Although clay contains phyllosilicates, it may contain other materials that impart plasticity and harden when dried or fired. Associated phases in clay may include materials that do not impart plasticity and organic matter" (Guggenheim et al., 2006).
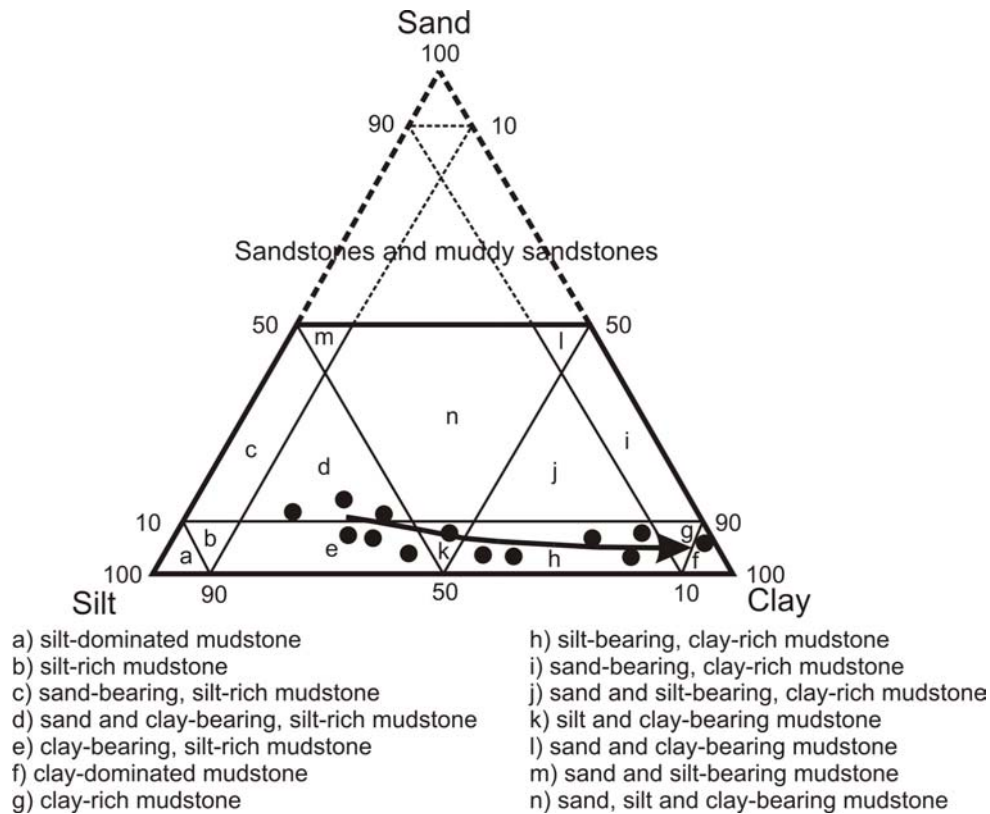
Fig. 1.1: Ternary diagram for the classification of mudstones with the end members sand, silt and clay (Macquacker & Adams, 2003). Examples for nomenclature are given in the legend. Arrow indicates mudstone types that might be present within an upward-fining succession.

Most clay minerals are water bearing alumosilicates with a platy shape and belong to the group of phyllosilicates. The basic structural units are [SiO$_4$]-tetrahedra (T) and [M(O,OH)$_6$]-octahedra (O), which are connected by shared oxygens.

Each tetrahedron is connected to three other tetrahedra, forming a sheet of hexagonal rings. The apical unshared corners of the tetrahedra point in a direction perpendicular to the tetrahedral sheet. The octahedra are edge-linked, also forming a sheet with hexagonal symmetry.

A distinction is drawn between 1:1 and 2:1 layersilicates. The 1:1-layer structure is build by one tetrahedral sheet and one octahedral sheet. In the junction plane, the apical oxygens of the tetrahedra also form two third of the octahedral corners. The octahedral corners, which are not linked to the tetrahedral sheets, are occupied by hydroxyl groups.

The 1:1 layersilicates include for example kaolinite and serpentine minerals (Fig. 1.2 a).

The 2:1-layer structure consists of so-called TOT-layers, whereas one octahedral sheet (O) is surrounded by two tetrahedral sheets (T) e.g. smectite (Fig. 1.2a).

The most frequent cation in the tetrahedra is silicon, which can also be substituted for by aluminum.

In the octahedral sheet, a distinction is drawn between di- and trioctahedral cation occupation. In dioctahedral sheets, two third of the octahedral positions are occupied, mainly by trivalent cations. In case of a trioctahedral structure, all octahedral positions are occupied by divalent cations.

The trivalent cations (Al^{3+}, Fe^{3+}) can partly be substituted by divalent cations (Fe^{2+}, Mg^{2+}), which leads to a negative layer charge.

In smectites, this charge ranges from 0.2 to 0.6 charges per formula unit and is compensated by cations in the interlayer space, e.g. Na^+, Ca^{2+} or Mg^{2+}. These interlayer cations are weakly bound and hydrated. Hydration in turn can lead to a widening of the distance between the TOT-layers (innercrystalline swelling).

Other 2:1-phyllosilicates belong to the talc-pyrophyllite group (layer charge per formula unit (LCFU) = 0), vermiculite (LCFU 0.6 – 0.9), illite (LCFU 0.6 – 0.9) or mica (LCFU = 1), respectively.

Chlorites have an additional octahedral sheet (di- or trioctahedral) in the interlayer space instead of exchangeable cations. Per definition, they belong to the 2:1-layer minerals. Formerly they were referred to as TOTO, or 4-layer minerals.
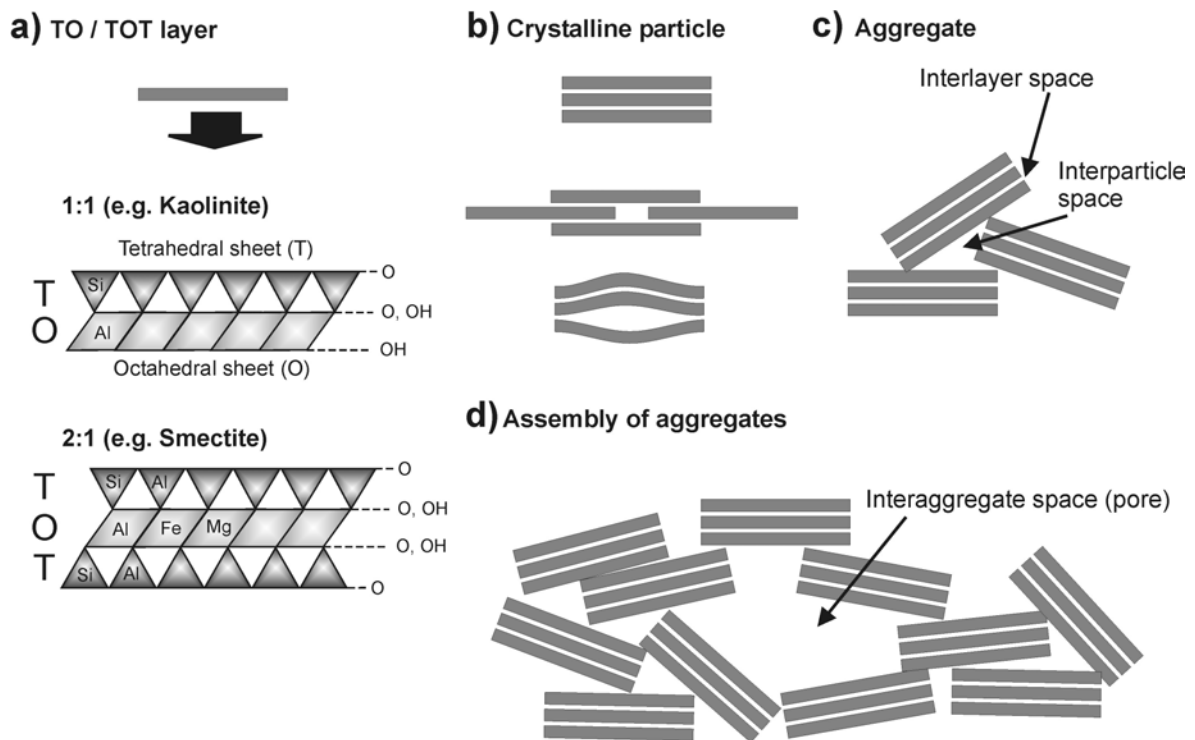

Fig. 1.2: a) basic unit of a clay mineral, TO- or TOT-layers **b)** crystalline particles made up of stacked TO- or TOT-layers. Lenticular pores arise from layer translation and deformation. **c)** aggregate made up of crystalline particles **d)** assembly of aggregates enclosing interaggregate space (Fig. modified according to Bergaya & Lagaly, 2006).

Several TO- or TOT-layers, respectively, build up crystalline particles which consist of up to 100 layers depending on the mineral. Smectite crystals may have on average less than 5 layers. Lenticular pores may arise from layer translation and deformation (Fig. 1.2 b). Crystalline particles built up non cemented aggregates with interparticle spaces (Fig. 1.2 c). In between such aggregates interaggregate spaces (pores) exist (Fig. 1.2 d).

Clays can be classified according to their clay mineralogical composition:

Kaoline mainly consists of clay minerals of the kaolin group (kaolinite, halloysite, nacrite and dickite).

Swelling clay minerals of the smectite group (montmorillonite, beidellite, nontronite) are main components of bentonites.

Common clays (clastic sediments) contain many different minerals owing to their different sedimentary histories. The main clay minerals are illite, and kaolinite, with admixtures of chlorite, smectite and mixed layered minerals.

In soil science non-silicate minerals of the clay fraction also belong to the group of the clay minerals, e.g. low crystalline Al- and Fe-(hydr)oxides.

1.2.   Mechanical behaviour of clay-stones

The anisotropic mechanical behaviour of clay-stones is controlled by the internal structure of the rock and the clay-electrolyte system. From the mechanical point of view clays are difficult to characterize because of their relative high porosity, swellable minerals, and the high deformable rock matrix. A simple characterisation of the behaviour is not possible due to coupled processes.

The mechanical characteristics of Opalinus Clay (northern Switzerland) were investigated by Nüesch (1991). Deformation experiments (coaxial and simple shear configurations) were conducted on undeformed Opalinus Clay samples from a borehole in the Jurassic Mountains. Nüesch investigated the influence of aggregate size, mineralogical composition, and water content on the deformation and concluded that cataclastic flow represents the main deformation mechanism.

Many studies about the mechanical behaviour and microfabric are focused on clay-stones of the Callovo-Oxfordian (Meuse/Haute Marne) and Toarcian formation (Tournemire). The Callovo-Oxfordian formation is a potential host rock for radioactive waste in France, and the Toarcian formation is investigated as a model system.

Bauer-Plaindoux et al. (1998) proved that mechanical properties and swelling do not only depend on the quantity and the nature of the clay but also on the material structure and texture. They observed that clays with comparable calcite contents can

have very different physical and mechanical behaviour. Accordingly they assumed that considering the calcite and clay arrangement (granulometry and intergranular cementation) could provide very useful information.

Chiarelli et al. (2000) investigated the influence of the mineralogical composition and moisture content on mechanical behaviour of Callovo-Oxfordian clay-stone and concluded that the rocks become more brittle and stiffer if the calcite content increases. Consequently, increasing clay content leads to a more ductile behaviour and increased plasticity. With decreasing moisture content the material becomes more brittle. Two mechanisms were identified: plasticity induced by slip of clay sheets and induced anisotropic damage as indicated by microcracks at the interface between grains and matrix.

The time-dependent mechanical behaviour of Oxfordian clay-stones from eastern France, Toarcian clay-stones from Tournemire, and marls from the Jurassic Mountains was investigated by Fabre & Pellet (2006). After mechanical testing, thin sections of the samples were analysed indicating cataclastic and granular creep. In addition, cracks were observed in the matrix but not in quartz or carbonate grains (with diameters about approximating 100 µm). Iron sulphides as framboidal pyrite aggregates (up to several mm) are considered as zones of weakness, and hence control the initiation and propagation of cracks in Oxfordian clay-stones.

Fouché et al. (2004) investigated two different horizons of the Callovo-Oxfordian formation. They performed plane deformation tests under compressive uniaxial loading, controlled humidity, and temperature. Microfabric changes were observed simultaneously using scanning electron microscopy (SEM). The authors claim that the clay content controls the deformability, that the bedding represents predetermined weakness surfaces, and that carbonates, quartz, and pyrite aggregates control the opening of fissures. Using numerical modelling it was possible to reproduce the deformation, to quantify the influence of a local heterogeneity, and to explain the differences between the real test and the numerical test by the role of structure and texture during its deformation. They conclude that the weathering of pyrite plays an important role and should be regarded as a supplementary cause of damage.

Oxidation is associated with crystallisation pressure during formation of secondary minerals. Charpentier et al. (2001) investigated the mineralogical evolution of clays in dehydrated-oxidised zones of the clayey walls of the Tournemiere tunnel (France). The secondary pyrite corrosion products - induced by atmospheric oxygen in the presence of adsorbed water - are minerals like gypsum, celestite, jarosite, and Fe-hydroxides. Oxidation processes have pronounced influence on the water-rock equilibria of the mechanically disturbed zone (EDZ).

Further changes in the fabric may result from unloading of the clay rock during sampling. Stress relaxation may lead to core discing parallel to bedding. Such microcracks significantly reduce the strength parallel to bedding (Nagra, 2002).

Repeated drying and rehydration leads to fabric changes, too. During drying of fine grained rocks, capillary forces are affecting the rock and which finally leads to loosening. Capillary forces are much stronger than the forces initially present in the clay-stones caused by over-consolidation e.g. by ice load (Einsele, 1983). Rehydration causes swelling and disintegration. Swelling can be divided into two major processes, intracrystalline swelling and intercrystalline/osmotic swelling (Heim, 1990). Intracrystalline swelling is ascribed to hydration of interlayer cations, while osmotic swelling is ascribed to different ion concentrations near the clay mineral surface in the pore water. Six mechanisms controlling the swelling of smectites in aqueous systems were identified by Laird (2006): "Crystalline swelling, Double-layer swelling, Formation and breakup of quasicrystals, Cation demixing, Co-volume swelling, and Brownian swelling".

The influence of large quartz and mica particles on the strength of "bentonite-treated petroleum wastes incorporated kaolinitic clay ceramics" was investigated by Monteiro et al. (2006). Their study demonstrates that these larger particles decrease the strength.

The present study is focused on the investigation of the microfabric of Opalinus Clay. Besides the content of carbonates, grain size and distribution of carbonates are assumed to influence the mechanical behaviour of clays. Accordingly, parameters like grain size and grain shape of carbonates are determined and compared with the mechanical parameters. To determine these parameters image analysis is used. The use of conventional methods for the determination of grain size distribution like disaggregation, sieving and sedimentation leads to dissolution of carbonates and is therefore not recommended.

For comparison and to verify the results, samples of the Callovo-Oxfordian formation are investigated as well.

2   Methods

2.1.   Mineralogical characterisation

The quantitative mineralogical composition was determined based on the qualitative analysis of the samples by XRD followed by quantification of x-ray pattern using the Rietveld method (Rietveld, 1967). Afterwards the results were refined using chemical data (XRF, TC, TS) as well as CEC and IR.

X-ray diffraction (XRD) and quantification by Rietveld method: Diffraction patterns were obtained either by a Phillips PW 3710 diffractometer (CuK$_\alpha$-radiation, Bragg-Brentano-geometry, fixed slits, secondary monochromator, point detector) or a Seifert 3003 TT diffractometer (CuK$_\alpha$-radiation, Bragg-Brentano-geometry, automatic slit, secondary monochromator, point detector). Measurements were carried out in reflection geometry using powdered samples < 20 µm. For quantification the Autoquan$^\circledR$ software (Taut et al., 1998) was used. Disordered phyllosilicates are described by appropriate disorder models (Bergmann & Kleeberg, 1998, Ufer et al., 2004).

X-ray fluorescence (XRF): Powdered samples were analyzed using a PANalytical Axios and a PW2400 spectrometer. Samples are prepared by mixing with a flux material and melting into glass beads. The beads are analyzed by wavelength dispersive x-ray fluorescence spectrometry (WD-XRF). To determine loss on ignition (LOI), 1000 mg of sample material are heated to 1030 °C for 10 min. After mixing the residue with 5.0 g lithium metaborate and 25 mg lithium bromide, it is fused at 1200 °C for 20 min. The calibrations are validated by analysis of reference materials. "Monitor" samples and 130 certified reference materials (CRM) are used for calibration and quality management.

Cation exchange capacity (CEC): The CEC was measured based on the Cu-Triethylenetetramine method (modified after Meier & Kahr, 1999). 50.0 mL of deionised water and 10.0 mL of 0.01 M Cu-Triethylenetetramine solution were added to the sample. Afterwards samples were shaken in an end-over-end shaker for two hours und finally centrifuged. The extinction of the supernatant was measured by VIS spectroscopy (wavelength 578 nm). Exchangeable cations were measured by ICP-OES.

Leco carbon and sulphur: The total carbon content (TC), the total sulphur content (TS) and the organic carbon content were measured with a LECO CS-444-Analysator. Samples of 170-180 mg of the air dried material were used to measure the total carbon and sulphur content simultaneously. The samples were heated in the device to 1800-2000 °C in an oxygen atmosphere, and the C and S were expelled as CO_2 and SO_2, which were detected with an infrared detector.

The organic carbon content was determined by the LECO oven after dissolution of the carbonates. Carbonates have been removed by treating the samples several times at 80 °C with HCl until no further gas evolution could be observed. Thereafter the samples were heated in the LECO device as described above.

Determination of carbonate content by Scheibler method: The determination of the carbonate content was carried out by a computerised method based on the Scheibler method (Klosa, 1994). 10 mL ca. 10 % hydrochloric acid were added to the sample in a 500 mL pressure vessel and the CO_2 pressure was measured. The results were used to check the Rietveld results.

Infrared spectroscopy (IR spectroscopy): Spectroscopic investigation of the mid infrared region (400-4000 cm^{-1}) was carried out using a Nexus FTIR spectrometer from Thermo Nicolet (beam splitter: KBr, detector: DTGS TEC). KBr pellets (1 mg sample diluted in 200 mg KBr) were measured in transmission mode.

2.2.   Optical characterisation

2.2.1   Scanning electron microscopy (SEM)

The SEM investigation was performed by using the environmental scanning electron microscope Quanta 600 F (field emission cathode) from FEI. The microscope is equipped with the EDS-system Genesis 4000 (EDAX) used for qualitative and quantitative (depending on preparation and measurement conditions) investigation of the chemical composition of the sample. The measurements were carried out in low-vacuum mode at 0.6 mbar. When using this mode a sputtering of the samples with gold or carbon is not necessary. For image analysis backscattered electron (BSE) images were used. Bright colours indicate heavy elements (e.g. Fe), whereas dark areas indicate light elements (e.g. C). By using the MLA® software (Mineral Liberation Analyser) an automatic measurement of BSE-images covering the whole polished section is possible.

2.2.2   Image Analysis

For image analysis BSE-images of polished sections were collected at a magnification of 200 using the MLA® software (Gu, 2003). To adjust brightness and contrast, pyrite was chosen as a reference because pyrite is typically the brightest mineral within the investigated clay-stone samples. The grey level of pyrite was adjusted to 245 – 250 and the resin to 1 - 10. By this adjustment the whole grey level scale is covered in the BSE image under investigation. The minerals in the clay-stone (including carbonates) then can be extracted by grey level analysis. To cover the whole section single pictures were merged into a mosaic using Adobe Photoshop® software. Representative sections were chosen from the total mosaic and analysed by the software Image SXM® (developed from NIH Image, for Mac OSX; public domain: http://www.liv.ac.uk/~sdb/ImageSXM/). The detection limit of a particle according to the procedure applied is four pixels. Particles from the edges of the images are not taken into account. For Opalinus Clay samples the resolution is 1 px = 5.8 µm. To demonstrate the principle a typical BSE-image (Fig. 2.1a) of sample BLT 12/10 was selected for image analysis. Fig. 2.1b shows the extracted carbonate particles using ImageSXM. In Fig. 2.1b the number of objects for image analysis is too high and most of these particles are very fine grained carbonates. Therefore, these very small particles are filtered (median filter) out (noise reduction). The result is depicted in Fig. 2.1c which finally is used for microfabric analysis of the carbonate distribution (Fig. 2.1d).

In case of Callovo-Oxfordian clay samples the resolution had to be adjusted to 1 px = 1.5 µm due to the generally finer grain size of the carbonates. This grain size requires a different level of resolution to avoid errors: Fig. 2.2a shows the effect of

different resolutions of images of sample 22_05 on image analysis. Extracted carbonates of the image with lower resolution (as it was used for Opalinus Clay) are shown in Fig. 2.2b and with higher resolution in Fig. 2.2c. In Fig. 2.2b many fine-grained particles were not considered. Coarser grains are fragmented due to filtering which significantly affects grain size distribution of the carbonates. Hence, the adjustment of resolution to 1.5 µm is required as these errors are avoided hereby. On the other hand, this high resolution is not suitable for Opalinus Clay samples because using this resolution would reduce the size of the image. Consequently coarser grains would touch edges and hence would not be considered. The results would not be representative.

In the final stage the extracted particles are analysed by software operation with respect to the following parameters: area, the longest and shortest axis of an ellipse (surrounding particle), perimeter, and the angle to horizontal (longest axis). From this data the aspect ratio of each particle (longest axis/shortest axis of the surrounding ellipse) can be calculated. For the grain size distribution the longest axis was used as the size parameter.
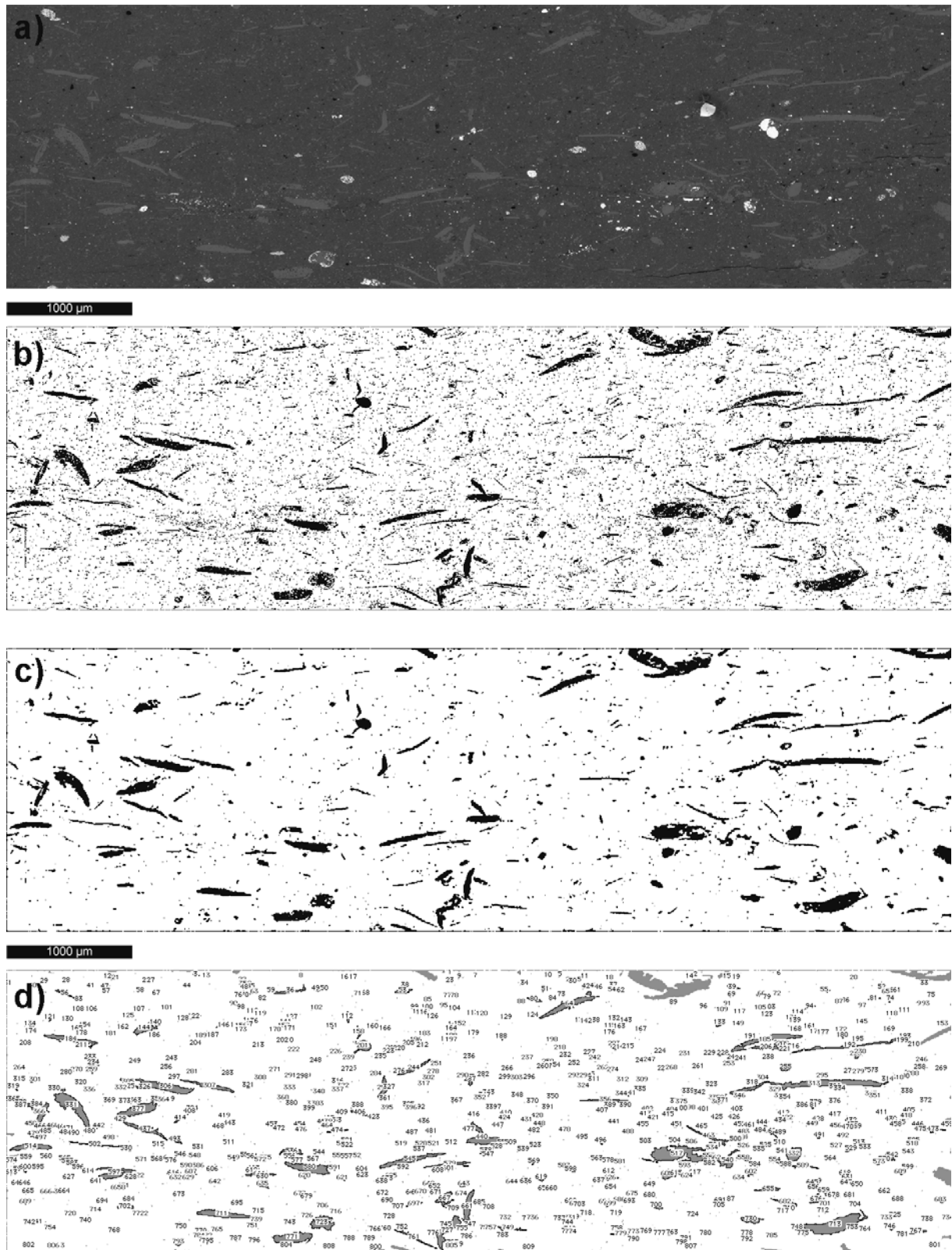
Fig. 2.1: Image analysis of Opalinus Clay BLT 12/10 **a)** BSE-image **b)** extracted particles **c)** extracted particles after filtering (median filter) **d)** analysed particles, numbered and outlined.
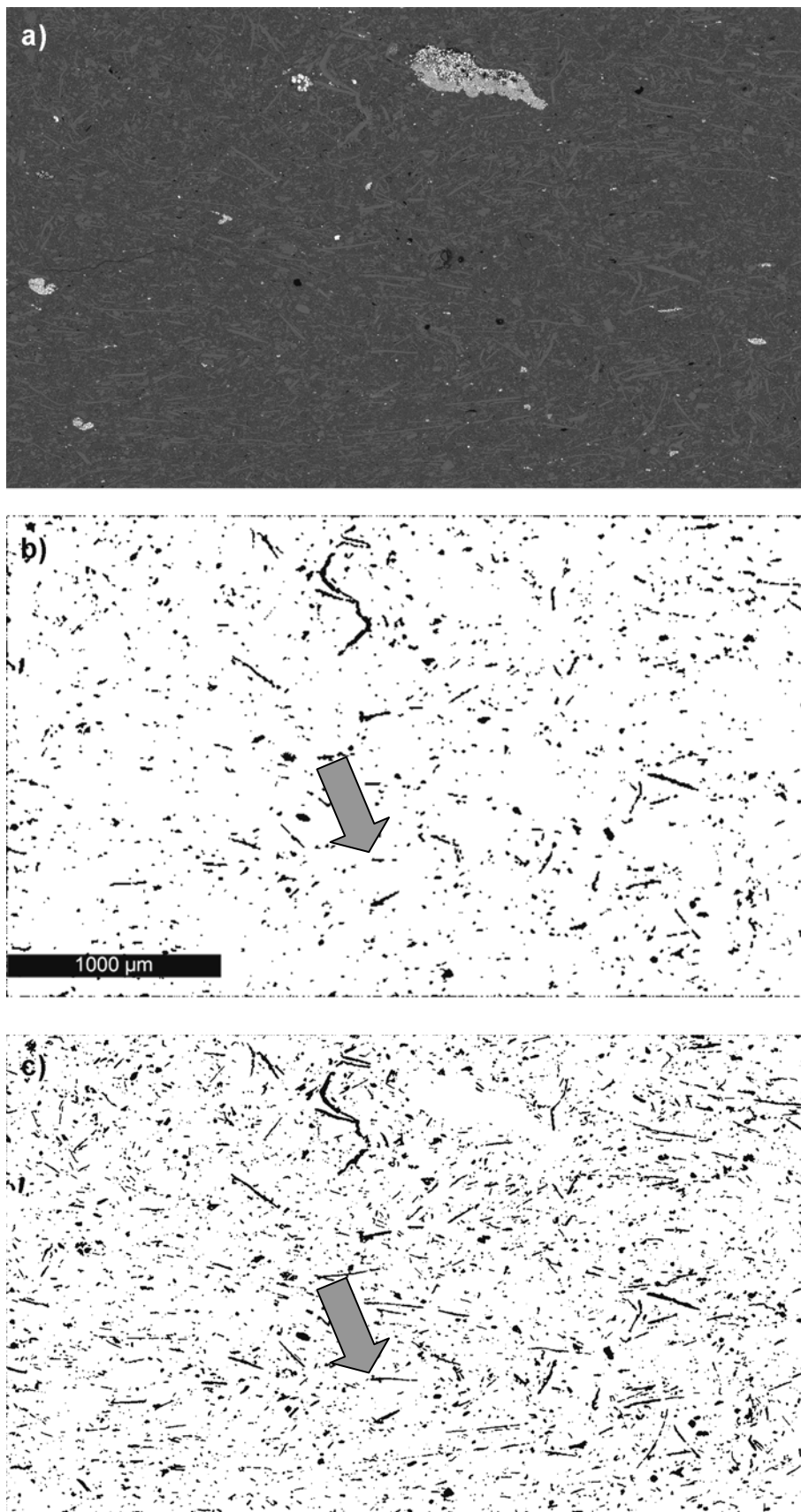
Fig. 2.2: Processing an image of Callovo-Oxfordian clay-stone (22_05) for fabric analysis: **a)** BSE-image **b)** extracted carbonates after filtering, image with low resolution (1 px = 5.8 µm) **c)** extracted carbonates after filtering, image with high resolution (1 px = 1.5 µm). The arrow marks a position where artefacts are produced by low resolution.

2.3.   Mechanical characterisation

The performance of uniaxial and triaxial compression tests is described by Schnier (2004) and Schnier & Stührenberg (2006). Cylindrical samples with a diameter of 92 to 101 mm and a length of 190 to 250 mm were used for the tests. The orientations of the core samples were parallel (p-samples), perpendicular (s-samples), and oblique at approximately 45 ° (z-samples) to the bedding. The tests were carried out at room temperature, 80 °C, and 120 °C. For s-samples different mechanical behaviour was observed, hence only s-samples were considered for the investigation of the microfabric.

True triaxial tests were performed on cubic samples (edge length 53 mm) of the Callovo-Oxfordian clay-stone from Meuse/Haute-Marne URL, France by Naumann & Plischke (2005).

3   Materials

3.1.   Opalinus Clay

In the last decades the Opalinus Clay in the north of Switzerland was investigated in detail due to its role as potential host rock for high level radioactive waste. Many investigations of the Opalinus Clay were performed in the URL Mont Terri which is located at the security gallery of a motorway tunnel near St. Ursanne (Thury, 1997, Thury & Bossart, 1999, Heitzmann & Bossart, 2001). The geological setting is given in Fig. 3.1.
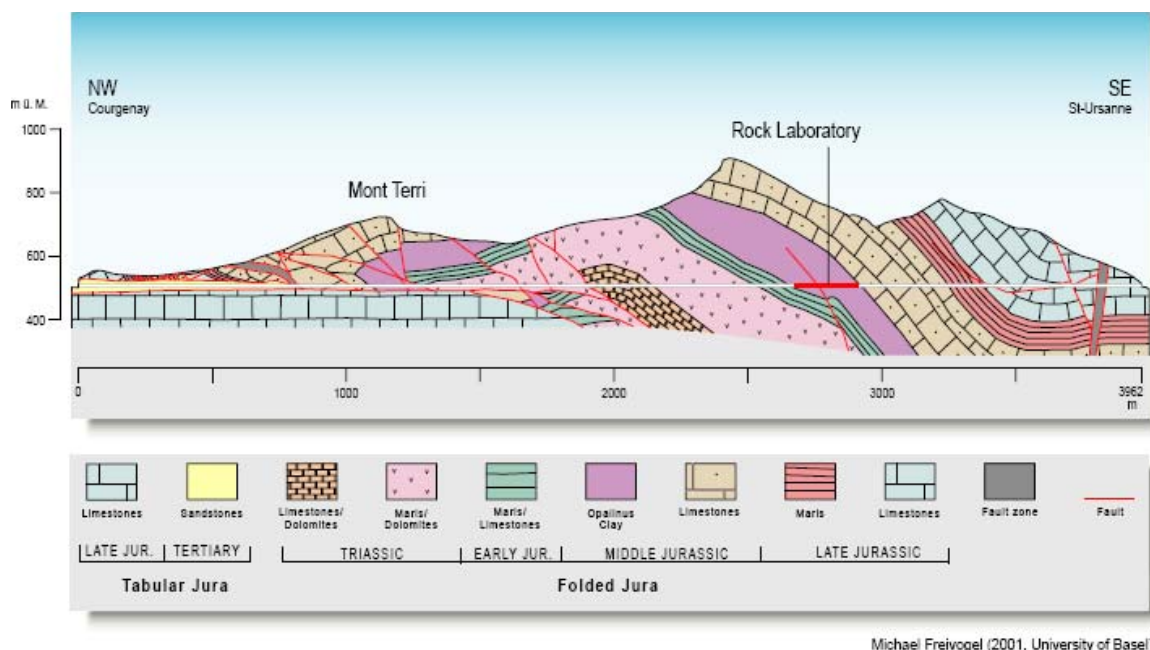
Fig. 3.1: Geological cross-section of the URL Mont Terri, Freivogel & Huggenberger (2003).

Mineralogy

The quantitative mineralogical composition of Opalinus Clay is relatively homogeneous on the dm-scale. The mineralogical composition was investigated in detail e.g. by Nagra (2002) and Kaufhold et al. (2004). The following minerals were detected in these studies: calcite, dolomite/ankerite, siderite, quartz, albite, K-feldspar, pyrite, illite, illite/smectite-mixed layer minerals, chlorite, kaolinite, rutile, goethite, and gypsum. The content of organic carbon is on average 1 wt.%.

The lower part of the Opalinus Clay formation is rich in clay minerals and is overlain by sandy and calcareous units. The mineralogical composition of samples from Mont Terri and Benken is similar, the clay content being higher at Mont Terri (Nagra,

2002). A pronounced variability of the ratios of clay minerals to carbonates and quartz at the meter to decametre scale is reported. Fissures mostly occur close to the surface (Nagra, 2002).

The millimetre to decimetre scale is characterised by a lamination which is characterized by the alignment of the clay minerals. This lamination causes anisotropies of hydrogeological, rock mechanical as well as transport properties. Heterogeneities like silt (lenses) and sand rich layers and concretions of siderite parallel to the bedding have a dimension of cm in vertical direction and dm in horizontal direction. Further sedimentary structures as hardgrounds and bioturbation occur (Nagra, 2002).

The micrometer to millimetre scale corresponds to the grain sizes of the minerals of Opalinus Clay. The size of clay minerals ranges from < 0.1 µm to 10 µm, other silicates and the carbonate minerals have a size of 10 µm to 1 mm. Clay-rich areas do not contain diagenetic cements. The proportion of partially cemented areas is between 2 and 10 vol. % (Nagra, 2002).

At a scale of 1 to 100 nm clay minerals and pore water occur interacting with each other. Here, usually the causes for swelling, self sealing, failure and creep of the rock originate (Nagra, 2002).

3.1.1 Selection of samples

For microfabric analysis samples of bore holes BHE-B2 (Heater experiment HE-B) and BLT-12 (Laboratory Testing (LT) Experiment) from the URL Mont Teri (Switzerland) were selected (Tab. 3.1).

Tab. 3.1: Opalinus Clay samples.

BHE-B2	BLT 12
BHE B2/8	BLT 12/10
BHE B2/21	BLT 12/11
BHE B2/26	BLT 12/13
BHE B2/29	BLT 12/07
	BLT 12/08
	BLT 12/14
	BLT 12/15

For SEM investigation and EDS-Mapping of BHE-samples freshly broken pieces (perpendicular to the bedding) were prepared.

Fig. 3.2: Cylindric sample (BLT 12/10) after mechanical testing. Samples for mineralogical and optical investigations were taken from the labeled area.

After mechanical tests, samples for microfabric analysis of BLT 12 were taken perpendicular to the bedding from the fracture zone (Fig. 3.2). Polished sections were prepared using a dry polishing method to avoid artefacts caused by wetting and drying. Samples for mineralogical investigation are derived from the same area.

3.2.   Callovo-Oxfordian Clay-stone

The Callovo-Oxfordian clay-stones, which were investigated in this study, stem from the URL Meuse/Haute Marne in the East of France, close to the village of Bure which is 50 km to the west of Nancy. The Callovo-Oxfordian formation is part of the Paris Basin where especially limestones, marls, and clayey rocks were deposited. This sub-circular intratectonic basin is bordered by the Ardennes to the northeast, the Vosges to the east, the Morvan to the southeast, the Massiv Central to the south and the Armorican Massif to the west (Gaucher et al., 2004). The eastern part of the Paris Basin is characterised by cuesta morphology, resulting from a westward dipping monoclinal structure. In the area of the URL the Callovo-Oxfordian clay-stone is up to 130 m thick in a depth between 400 and 500 m (Fig. 3.3).

The Callovo-Oxfordian clay-stone (C2) can be divided into four lithostratigraphic units (termed C2a to C2d) which vary in claymineral and carbonate content. (Gaucher et al., 2004).
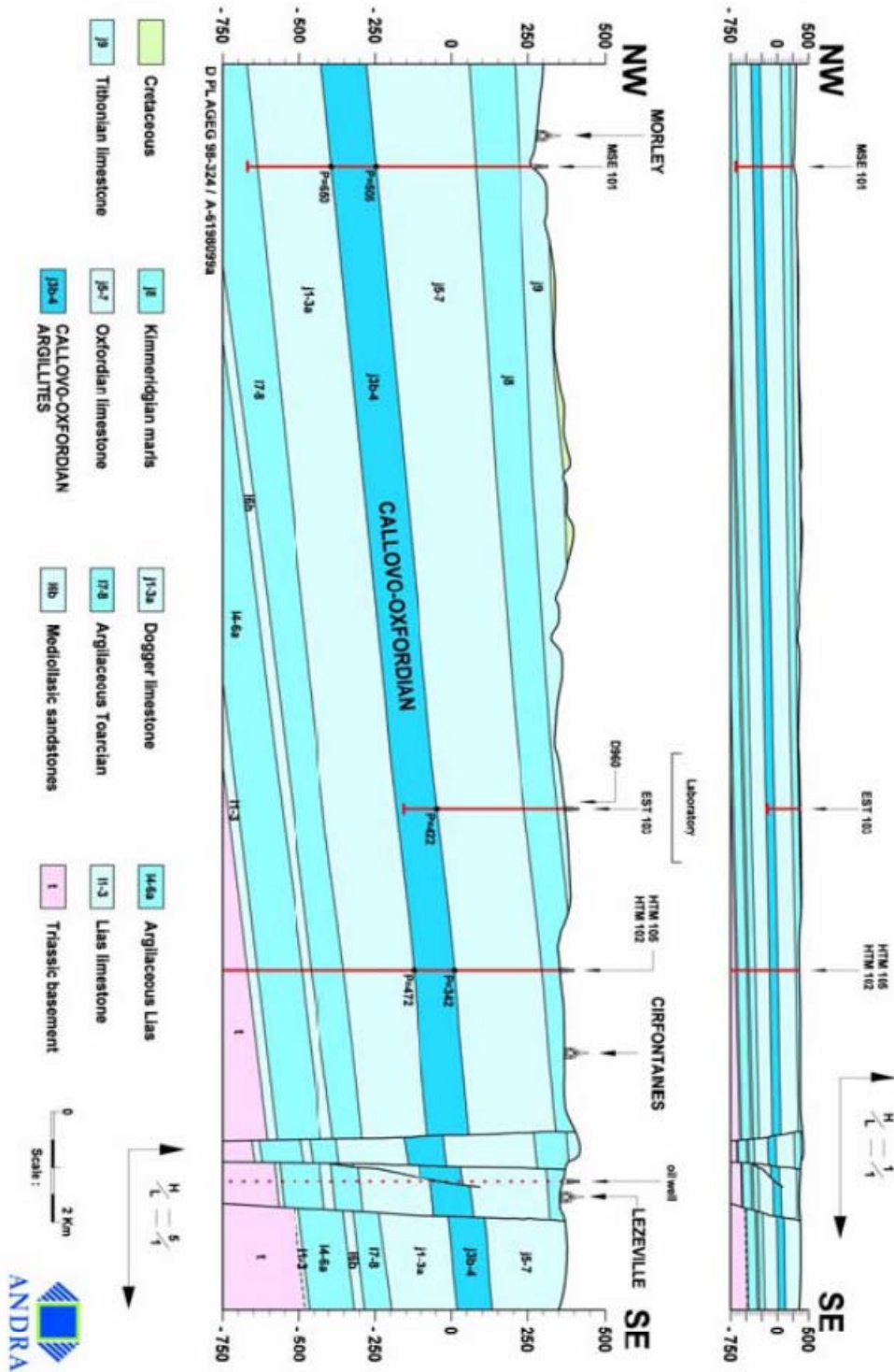
Fig. 3.3: Geological cross-section of the URL Meuse/Haute-Marne (ANDRA, 1999).

Mineralogy

The clay mineral composition of the Callovo-Oxfordian clay-stone is described in detail by Gaucher et al. (2004) and given in Tab. 3.2.

Tab. 3.2: Mineralogical composition of Callovo-Oxfordian clay-stones (wt. %), taken from Gaucher et al., (2004).

Minerals			C2b1				C2b2	C2c	C2d	
			Total	Below the MCZ	MCZ	Above the MCZ			Without carbonate bed	Total
Illite group		Min	9	17	16	9	10	2	6	2
		Max	21	21	19	13	15	19	8	8
		Avg.	16	20	17	11	13	12	7	6
Interstratified illite-smectite	Disordered I/S_{R0}	Min	0	0	25	28	24	4	7	3
		Max	33	0	30	33	29	32	23	23
		Avg.	16	0	27	31	27	18	15	13
	Ordered I/S_{R1}	Min	0	20	0	0	0	0	0	0
		Max	24	24	0	0	0	0	0	0
		Avg.	10	22	0	0	0	0	0	0
Kaolinite		Min	1.4	3.4	1.4	1.4	1.4	0	0	0
		Max	5	5	3.9	1.5	1.5	1.4	0	0
		Avg.	3	4.4	2.6	1.5	1.4	0.2	0	0
Chlorite		Min	1.9	2.4	2	1.9	1.4	1.5	0	0
		Max	2.7	2.7	2	2	2.4	2.4	1.5	1.5
		Avg.	2.2	2.6	2	2	1.9	1.9	1.1	0.9
Quartz		Min	17	17	21	23	23	10	32	17
		Max	27	21	22	27	32	43	36	36
		Avg.	22	19	22	25	26	26	34	30
Calcite		Min	17	20	20	17	11	12	26	26
		Max	24	23	20	24	25	75	43	73
		Avg.	21	22	20	21	21	32	33	41
Dolomite/ankerite		Min	2	3	2	2	2	2	2	2
		Max	6	6	3	4	8	8	8	8
		Avg.	3	4	3	3	5	4	6	5
Potassic feldspars		Min	1.9	1.9	1.9	1.9	1.8	0.9	1.0	1.0
		Max	2.1	2.1	1.9	2.0	1.9	2.8	1.0	1.0
		Avg.	2.0	2.0	1.9	1.9	1.9	1.8	1.0	1.0
Plagioclases		Min	0.9	1.0	1.0	0.9	0.9	0.9	1.0	1.0
		Max	1.1	1.1	1.0	1.0	1.0	1.0	1.4	1.4
		Avg.	1.0	1.0	1.0	1.0	0.9	0.9	1.1	1.1
Pyrite		Min	0.5	0.5	0.8	0.5	0.5	0.2	0.3	0.2
		Max	0.9	0.8	0.8	0.9	0.9	0.9	0.7	0.7
		Avg.	0.7	0.7	0.8	0.7	0.7	0.7	0.5	0.4
Siderite+ferriferous minerals		Min	1.4	1.9	1.9	1.4	1.4	0.5	0.5	0.5
		Max	2.7	2.7	1.9	1.9	1.5	1.5	1.4	1.4
		Avg.	1.9	2.2	1.9	1.6	1.4	1.1	1.0	0.9
Titanium minerals		Min	0.1	0.1	0.3	0.3	0.2	0	0.1	0.1
		Max	0.4	0.4	0.3	0.3	0.3	0.3	0.2	0.2
		Avg.	0.3	0.3	0.3	0.3	0.3	0.2	0.1	0.2
Phosphate minerals		Min	0.2	0.2	0.2	0.2	0.2	0.2	0.2	0.2
		Max	0.6	0.3	0.2	0.6	0.2	0.2	0.2	0.3
		Avg.	0.3	0.3	0.2	0.3	0.2	0.2	0.2	0.2

3.2.1 *Selection of samples*

Two samples of the Callovo-Oxfordian clay-stone, which differ in carbonate content were investigated (Naumann & Plischke, 2005). They are derived from boreholes SUG 1118 (borehole depth 19.43 m, sample 22_05; EST22216/01) and SUG 1105 (borehole depth 7.93 m, sample 23_05; EST22236/03). Boreholes were drilled in a vertical direction from the main level at 490 m depth. For electron optical investigations (including microfabric characterization), polished sections were prepared after mechanical testing.

Two further samples of the Callovo-Oxfordian clay-stone from borehole GIS 1002 (samples VL 7, EST25605; VL 8, EST25610) were selected and investigated with respect to the mineralogical composition, only.

4 Results

4.1. Mineralogical composition

Opalinus Clay

The results of the mineralogical analysis of Opalinus Clay of BHE-B2 and BLT 12 are given in Tab. 4.1. The contents of the different dioctahedral 2:1 layer silicates (illite, muscovite, smectite, and illite-smectite mixed layer minerals) are summed up, because a quantification of mixed layer minerals by the Rietveld method is not possible, yet.

Calcite was identified as the only calcium-carbonate mineral by XRD. Additionally, aragonite was identified using IR-spectroscopy (CO_3 vibration at 1480 cm^{-1}, Fig. 4.1). Since quantification by IR is difficult, the calcium carbonates are not differentiated quantitatively.
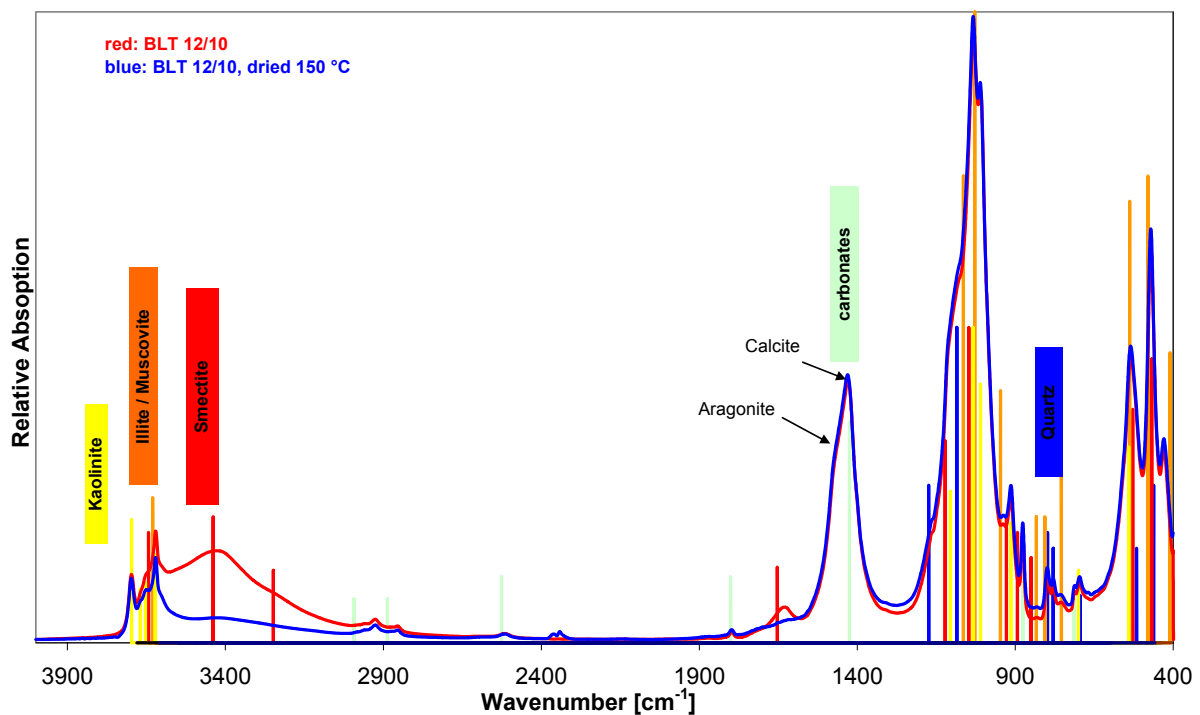
Fig. 4.1: IR-spectra of BLT 12/10 diluted in KBr. Red: before drying, blue: dried at 150 °C.

In general, the BHE samples considered for mineralogical investigation are derived from several cm long drill cores. As a result, smaller scale heterogeneities are averaged by the homogenising procedure. Hence, the variation of the carbonate content is relatively small (max. 3 wt. %). In case of the BLT samples, materials are taken from the fractured area of the drill cores after mechanical testing. They

represent smaller volumes and hence heterogeneities are larger (carbonate content: 8 -21 wt.-%). This confirms the results published in NTB 02-03 (Nagra, 2002). The results of the mineralogical analysis are given in Tab. 4.1.

Tab. 4.1: Mineralogical composition of Opalinus Clay samples of BHE-B2 and BLT 12

	BHE B2/8	BHE B2/21	BHE B2/26	BHE B2/29	BLT 12/07	BLT 12/08	BLT 12/10	BLT 12/11	BLT 12/13	BLT 12/14	BLT 12/15
Pyrite	3	3	2	2	3	2	3	4	**6**	2	2
Quartz	12	12	12	12	12	12	10	13	13	12	13
Gypsum	1	2	1	1	1	1	1	< 1	< 1	1	1
Calciumcarbonate	**12**	**13**	**14**	**15**	**17**	**16**	**20**	**10**	**6**	**8**	**10**
Siderite	2	2	3	2	2	2	2	2	2	2	2
2:1 dioc. layersilicates (Ill, Smt, Musc., Ill/Smt Mixed Layer)	33	31	31	31	30	31	30	33	36	35	34
Kaolinite	24	23	23	22	21	21	21	24	23	26	25
Clinochlore Mg/Fe	8	8	8	8	8	7	7	8	7	8	8
Na/Ca-Feldspar	1	2	2	2	1	2	2	1	1	1	1
K-Feldspar	3	3	3	3	2	3	3	3	3	4	3
Goethite	1	< 1	< 1	< 1	1	1	1	1	< 1	1	1
Anatase/Rutile	1	1	< 1	< 1	< 1	< 1	< 1	1	1	1	1
Apatite/APS	< 1	< 1	< 1	< 1	< 1	< 1	< 1	< 1	< 1	< 1	< 1
Sum Carbonates	**14**	**15**	**17**	**17**	**19**	**18**	**21**	**12**	**8**	**10**	**12**
CEC meq/100g	11	11	11	11	12	13	12	13	14	14	14

Callovo-Oxfordian Clay-stone

The results of the mineralogical analysis are given in Tab. 4.2. Among the Callovo-Oxfordian clay-stone samples, sample 22_05 has the highest carbonate content (45 wt. %). In all the other samples the carbonate content ranges from 22 to 26 wt. %. Kaolinite was detected by IR-spectroscopy in samples 22_05, VL7, and VL8. In sample 23_05 kaolinite is absent (Fig. 4.2). The amount of quartz and clay minerals vary according to the carbonate content. Other variations are comparably small.

Tab. 4.2: Mineralogical composition of Callovo-Oxfordian clay-stones.

	22/05	23/05	VL7	VL8
Pyrite	3	3	3	3
Quartz	12	19	20	20
Gypsum				
Calciumcarbonate	**38**	**23**	**16**	**16**
Siderite	1	< 1	1	1
Dolomite	6	3	5	4
2:1 dioc. layersilicates (Ill, Smt, Musc., Ill/Smt Mixed Layer)	31	45	47	46
Kaolinite	3		2	2
Clinochlore Mg/Fe	3	3	3	4
Na/Ca-Feldspar	1	2	1	1
K-Feldspar	2	1	2	2
Goethite	< 1	< 1	< 1	< 1
Anatase/Rutile	< 1	< 1	< 1	< 1
Apatite/APS	< 1	< 1	< 1	< 1
Sum Carbonates	**45**	**26**	**22**	**22**
CEC meq/100g	7	18	16	16
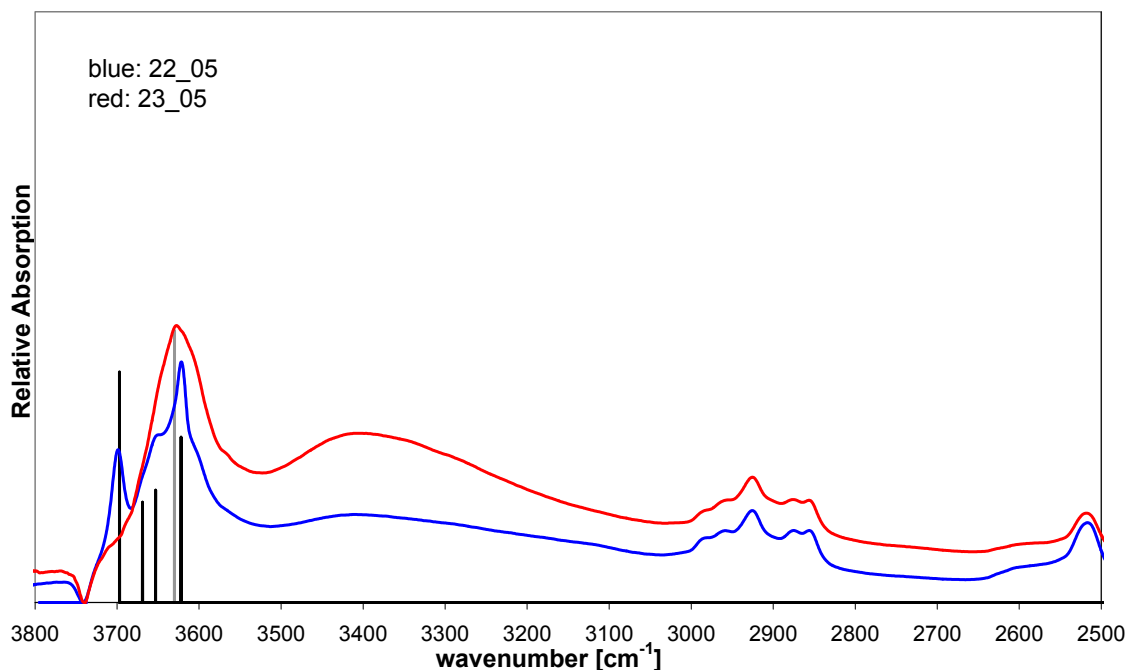
Fig. 4.2: IR-Spectra of samples 22_05 (red) und 23_05 (blue). Band positions of kaolinite (black), illite/muscovite (grey). Bands between 2800 – 3000 cm^{-1} correspond to carbonates and organic matter.

The main difference between the mineralogical composition of Opalinus Clay and Callovo-Oxfordian clay-stones are the qualitative and quantitative differences of the

individual clay minerals. In Opalinus Clay kaolinite varies between 20 and 25 wt. %, while its maximum concentration is 3 wt. % in Callovo-Oxfordian clay-stones. The chlorite content of Callovo-Oxfordian clay-stones is 3 wt. %, which is 5 wt. % lower as in Opalinus Clay. The content of 2:1 layer silicates in Callovo-Oxfordian clay-stones (31 – 47 wt. %) is higher on average compared to Opalinus Clay (30 – 36 wt. %). In addition, dolomite is present in Callovo-Oxfordian clay-stones (3 – 6 wt. %) but could not be detected in Opalinus Clay. Gypsum is only present in Opalinus Clay, likely representing a product of pyrite oxidation.

4.2.   Mechanical behaviour

Opalinus Clay

The mechanical behaviour of Opalinus Clay samples was investigated in the frame of the Heater Experiment project (HE-B) in Mont Terri (Göbel et al., 2007). A number of uniaxial and triaxial compression tests were performed on samples (Schnier, 2004) which are taken from HE-B bore holes. The orientations of the core samples were parallel (p-samples), perpendicular (s-samples), and oblique at approximately 45 ° (z-samples) to the bedding. The author identified two different types of Opalinus Clay with respect to mechanical properties: For s-samples two groups (high and low failure strength) could be distinguished. The observed differences were supposed to result from differences of the mineralogical composition (Schnier, 2004).
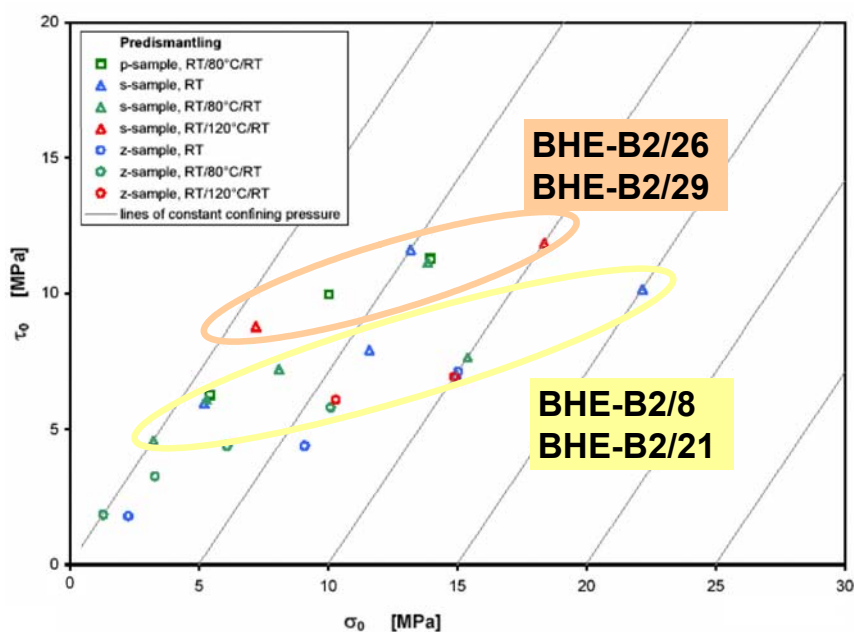
Fig. 4.3: Failure strength of BHE-B2 specimens in uni- and triaxial compression tests (Schnier, 2004).

In the frame of the LT-Experiment (URL Mont Terri, Switzerland) Opalinus Clay samples from bore holes BLT 12 and BLT 5 were investigated. Uni- and triaxial compression tests at different temperatures (room temperature and 80 °C) were carried out on s-samples (perpendicular to bedding) by Schnier & Stührenberg (2006). The failure strength values of samples tested at 80 °C are 20 to 25 % lower than those determined at room temperature (Fig. 4.4). In addition, the failure strength values of sample BLT 12 differ significantly compared to those of sample BLT 5. Samples BLT 12/08, BLT 12/07, and BLT 12/10 show comparatively lower failure strength values than BLT 12/11, BLT 12/13, BLT 12/14, and BLT 12/15.

Generally, the failure strength values decrease with increasing carbonate content. However, some exceptions have to be explained. It was assumed that considering the microfabric is helpful in these instances.
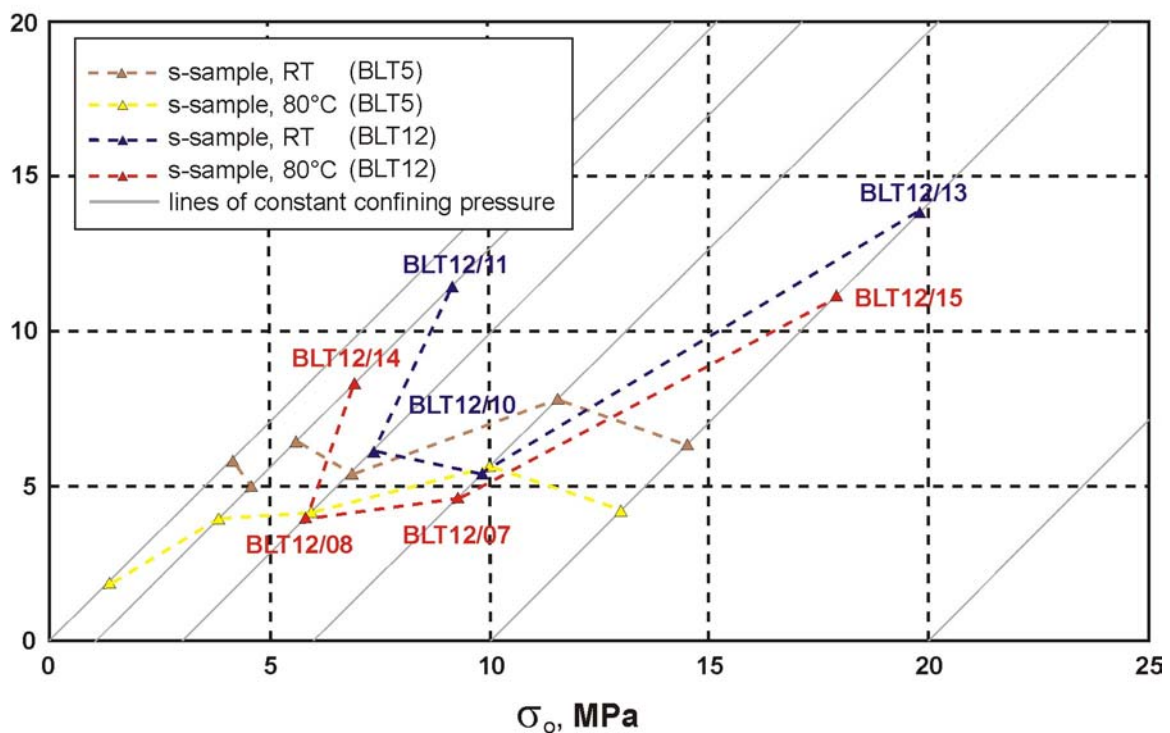
Fig. 4.4: Failure strength of BLT specimens (s-samples) in uniaxial and triaxial compression (figure taken from Schnier & Stührenberg, 2006).

Callovo-Oxfordian Clay-stone

True triaxial tests were performed on cubic samples of the Callovo-Oxfordian clay-stone from Meuse/Haute-Marne URL, France (Naumann & Plischke, 2005). The authors discuss the close correlation of higher failure strength values (Fig. 4.5) and stiffness (Fig. 4.6) in samples with higher carbonate content.
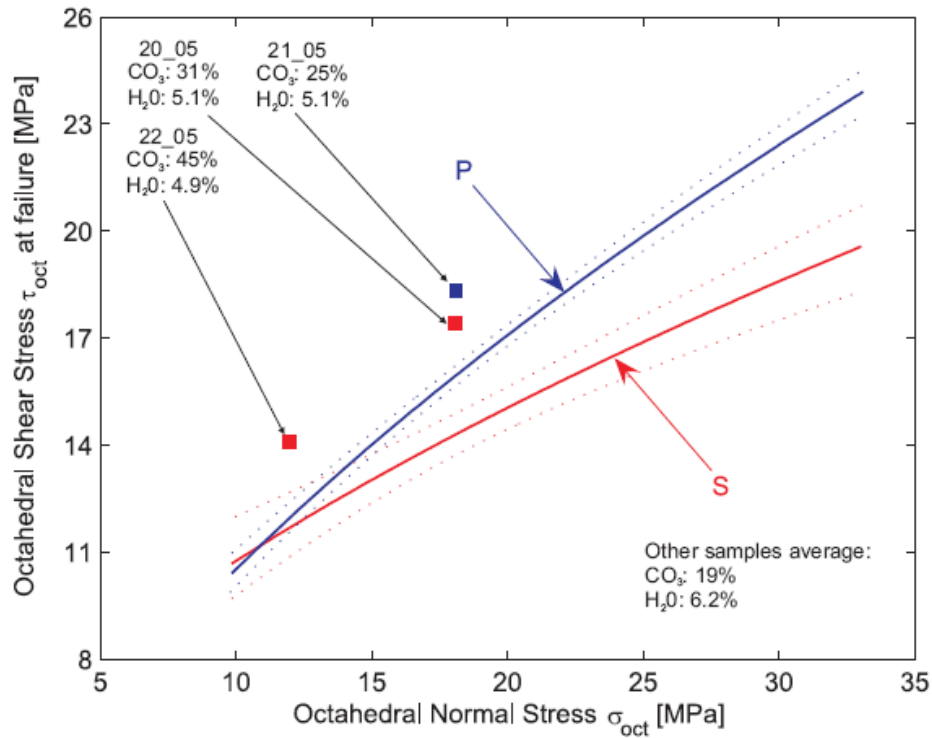
Fig. 4.5: Deviation of strength properties of specimens labelled with their known properties distinct from the majority of investigated samples. Octahedral plot of the Hoek-Brown-failure envelopes. Dotted lines represent confidence interval ± 1σ derived from the sets of fit parameters. Carbonate content = CO_3. Figure taken from Naumann & Plischke (2005).
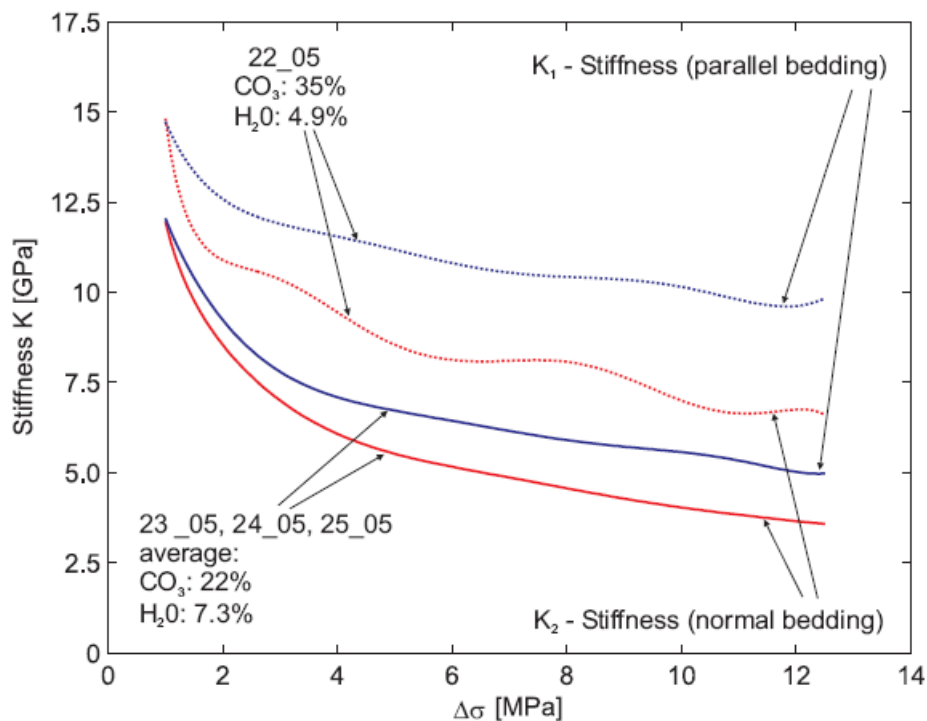
Fig. 4.6: Observed stiffnesses K1 and K2 during cyclic loading of sample 23_05 (results from three subsequent cycles). Mean values from two directions parallel to bedding represented in K1. Carbonate content = CO_3. Figure taken from Naumann & Plischke (2005).

The microfabric of sample 22_05 (carbonate content: 45 wt.-%) and sample 23_05 (carbonate content: 26 wt.-%) was investigated in detail. These samples were selected because their mechanical behaviour is different compared to Opalinus Clay samples: Generally, failure strength of Opalinus Clay decreases with increasing carbonate content while failure strength of Callovo-Oxfordian clay-stone increases.

4.3.   Microfabric / Carbonate distribution model

Opalinus Clay

The results of the microfabric investigation of Opalinus Clay show a clayey matrix with fine- to coarse-grained carbonate bioclasts (shell fragments) and small idiomorphic calcite crystals (Fig. 4.7 a). Framboidal pyrite aggregates are evident, reaching a size of several cm (Fig. 4.7 b). Pyrite also occurs as fine-grained idiomorphic single crystals.
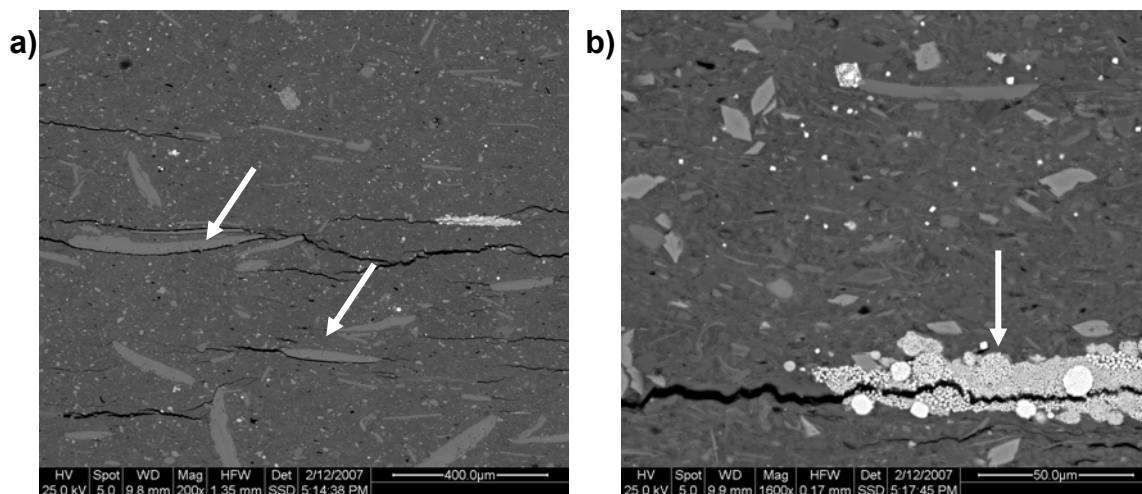
Fig. 4.7: SEM images (BSE) of polished sections of Opalinus Clay **a)** shell fragments (light grey, marked with arrows) in a clayey matrix **b)** framboidal pyrite (marked with arrow).

Fig. 4.8 a & b show SEM images of the > 63 µm fraction of sample BHE 1/19. The three-dimensional morphology of the coarse-grained particles can be observed. The carbonate shell fragments are platy with a smooth surface (Fig. 4.8 a). Fig. 4.8 b shows a coarse framboidal pyrite aggregate with a size of approximately 300 µm.
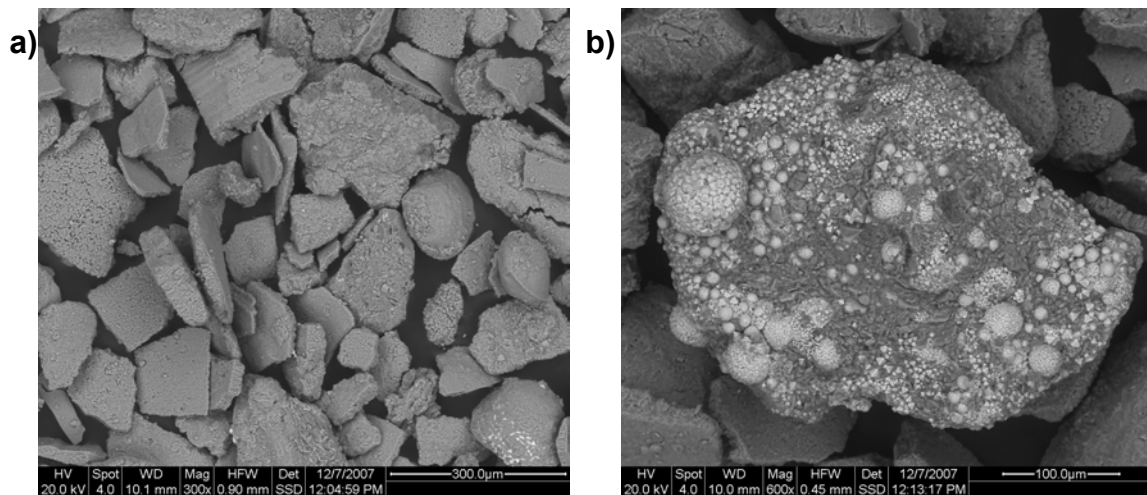
Fig. 4.8: BSE images of > 63 µm fraction of Opalinus Clay BHE 1/19 **a)** ± platy carbonate bioclasts (shell fragments) with a smooth surface **b)** framboidal pyrite aggregate.

The microfabric of the BHE samples was first studied on freshly broken drill core pieces (without polishing) after mechanical testing. Three adjacent areas (1 x 1 mm each) were chemically mapped using EDS. In Fig. 4.9 the sample BHE-B2/21 (lower failure strength, Fig. 4.9 a, c, e) is compared with the sample BHE-B2/29 (higher failure strength, Fig. 4.9 b, d, f). Two samples with comparable carbonate content were considered in detail, which significantly differ with respect to the mechanical strength. However, there is a significant difference: The sample with lower failure strength contains coarser grains whereas the sample with higher failure strength has a more homogenously distributed and much finer average grain size. Coarse grains in BHE-B2/21 are mainly carbonate bioclasts and pyrite (trace fossils). Carbonates and silicates were discriminated by the chemical mapping of Ca and Si (Fig. 4.9 c & d). Framboidal pyrite was identified by using the Fe distribution (Fig. 4.9 e & f) and confirmed by S mapping (not shown). In the sample with the more inhomogeneous texture, several cracks can be observed running along the discontinuities (marked with arrows in Fig. 4.9 a, b). The crack formation might be caused either by unloading, breaking of the sample, drying, and/or oxidation of pyrite, respectively. In case of sample BHE-B2/21 several cracks were observed. Based on Fig. 4.9 it can be tentatively concluded that the failure strength does not only depend on the content of carbonates but also on the shape, size, and spatial distribution of the carbonates. This observation is used as a model for the subsequent investigation of the LT samples (Laboratory Testing experiment, Mont Terri project). These samples also were selected because of strong variations in their failure strength values.
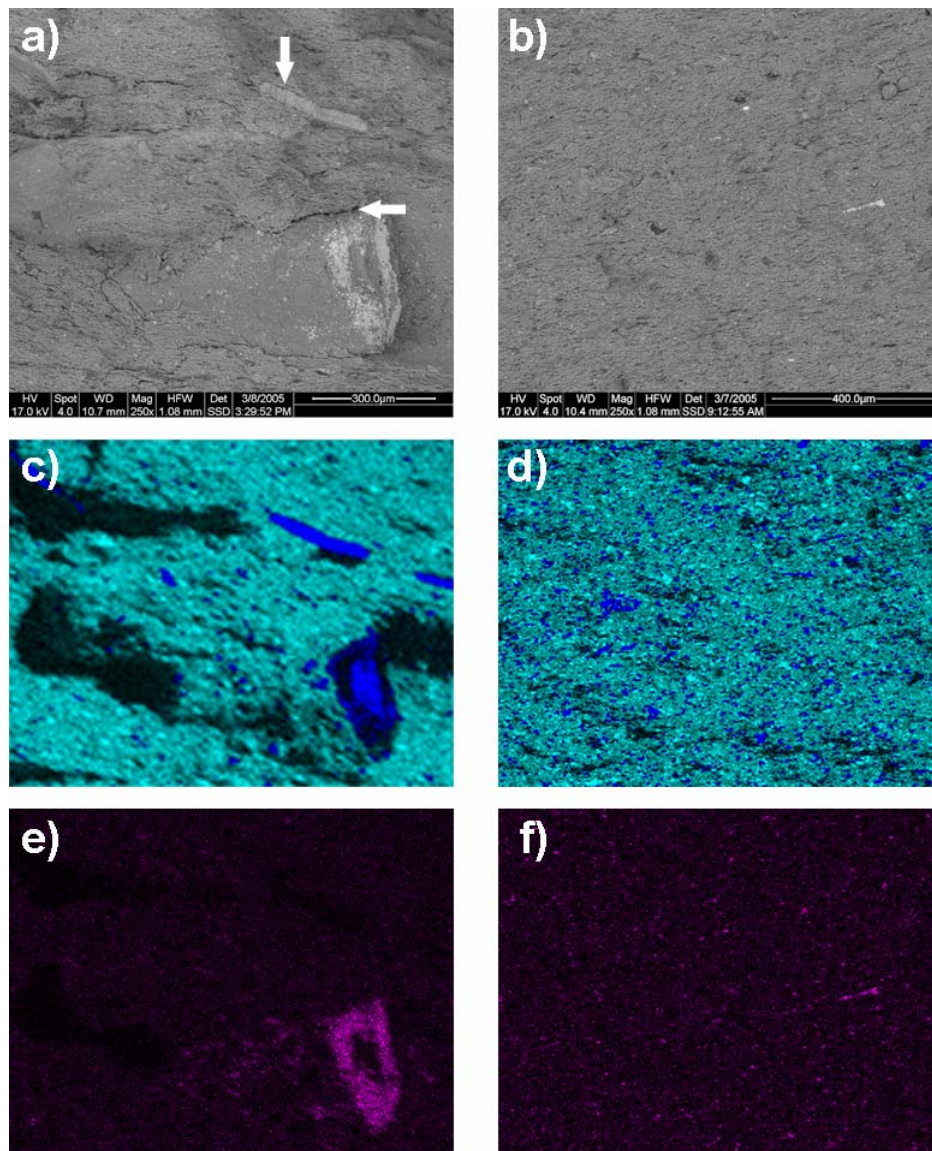
Fig. 4.9: BSE images of Opalinus Clay **a)** BHE-B2/21 (low failure strength). Arrows mark cracks running along discontinuities. **b)** BHE-B2/29 (high failure strength), **c)** EDS element distribution maps of Si (cyan) and Ca (blue) in BHE-B2/21 **d)** BHE-B2/29, **e)** element distribution of Fe in BHE-B2/21 and **f)** BHE-B2/29.

The images of BLT-samples prove that cracks occur at grain boundaries of the large and "smooth" shell fragments (Fig. 4.10). Commonly, they start at the edges of these fragments and continue into the clayey matrix, where they end or proceed to the next shell fragment. The cracks are partially filled with gypsum.
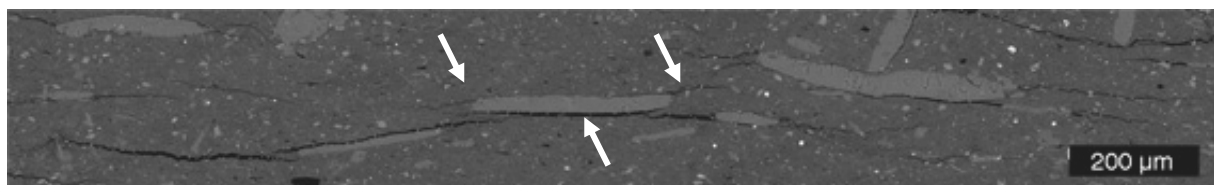
Fig. 4.10: Detail of a polished section of Opalinus Clay BLT 12/07. Shell fragments in clayey matrix. Cracks occurring at grain boundaries and edges of coarse shell fragments are marked with arrows.

Comparison of SEM-BSE-images and image analysis of clay-stones with different failure strength

In order to characterize Opalinus Clay samples with different failure strength values, BLT12/08 + BLT 12/14 and BLT 12/10 + BLT 12/11 were selected for further systematic investigation of the effect of microfabric on physical properties. The failure strength values of sample BLT 12/08 and BLT 12/10 are lower than those of samples BLT 12/14 and BLT 12/11 which were tested at 1 MPa confining pressure while BLT 12/08 and BLT 12/10 were tested at 3 MPa (Fig. 4.4) (Schnier & Stührenberg, 2006). Failure strength should increase with increasing confining pressure. However, the opposite was observed in samples BLT12/08 + BLT 12/14 and BLT 12/10 + BLT 12/11.

This observation can be explained by the carbonate-controlled microfabric results presented in Fig. 4.11.

Fig. 4.11 a & b show representative BSE-images of BLT 12/08 and BLT 12/14. Fig. 4.11 c & d illustrate the extracted carbonates of these images used for the quantification of the carbonate fabric. The content of coarse shell fragments in sample BLT 12/08 (low strength) is much higher than in sample BLT 12/14 (high strength). In contrast BLT 12/14 contains fine, spherical, and less elongated carbonates. In addition, cracks occur at the grain boundaries of carbonates running both parallel and perpendicular to the bedding in BLT 12/08 (as already observed in Fig. 4.10).

In order to validate the results presented yet, two additional samples were investigated. BSE-images and extracted carbonates of BLT 12/10 (low strength) and BLT 12/11 (high strength) are compared in Fig. 4.12. The content of carbonatic shell fragments is higher in BLT 12/10 (Fig. 4.12 a & c). The sample BLT 12/11 (Fig. 4.12 b & d) also contains coarse shell fragments but the distances between these particles are larger and accordingly they are isolated in the matrix. Accordingly, cracks end in the matrix. However, Fig. 4.12 confirms the conclusions drawn from Fig. 4.11.
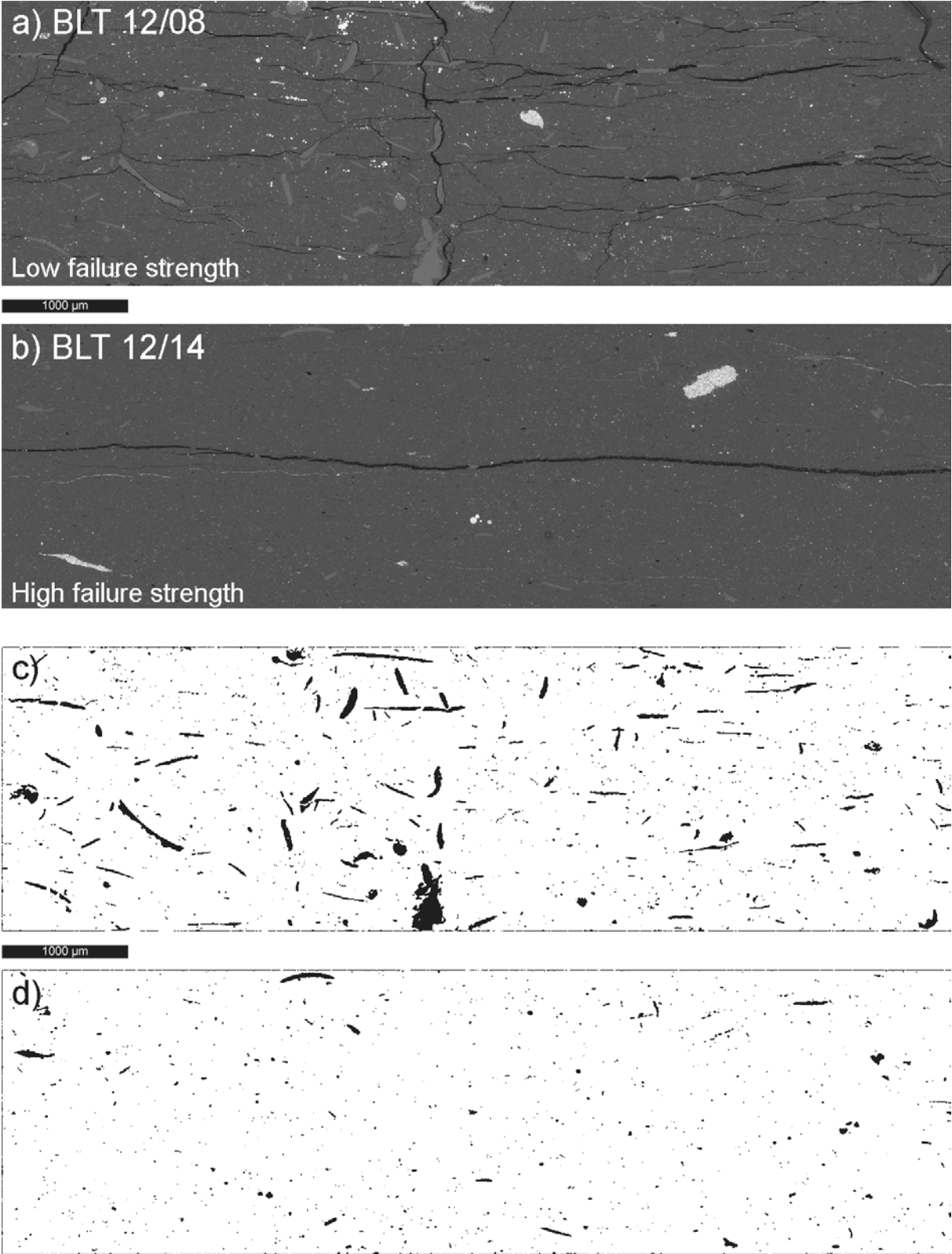
Fig. 4.11: Comparison of Opalinus Clay samples a) BLT 12/08, BSE-image (low failure strength) and b) BLT 12/14, BSE-image (high failure strength); c) extracted carbonates of BLT 12/08 and d) extracted carbonates of BLT 12/14.
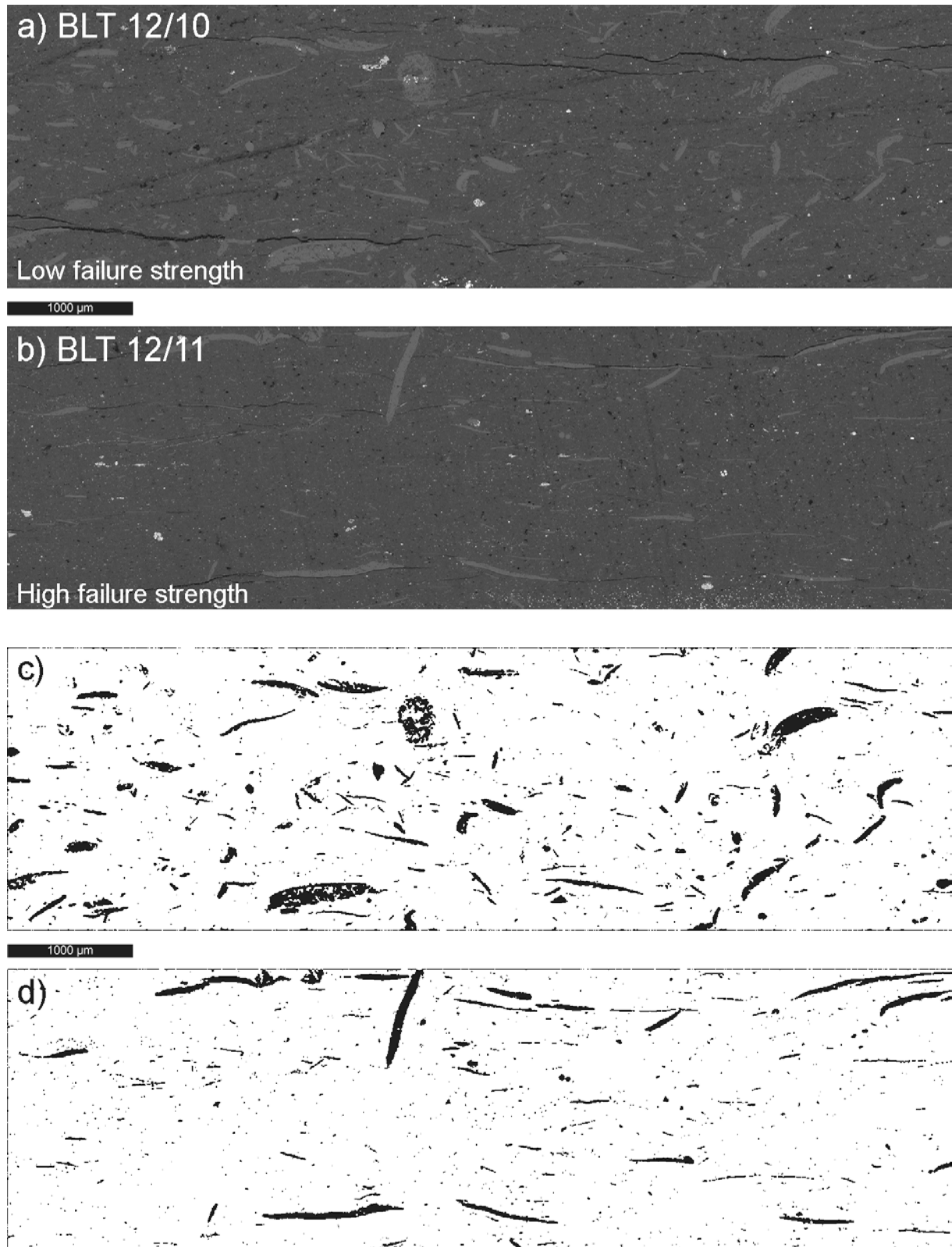
Fig. 4.12: Comparison of Opalinus Clay samples a) BLT 12/10, BSE-image (low failure strength) and b) BLT 12/11, BSE-image (high failure strength); c) extracted carbonates of BLT 12/10 and d) extracted carbonates of BLT 12/11.

Carbonates are oriented sub-parallel to the bedding as determined by image analysis (Fig. 4.13). Fig. 4.13 a shows the orientation of the longest axis with respect to the bedding versus the aspect ratio (longest axis / shortest axis) of BLT 12/08 and BLT 12/14. 2000 particles per sample were analyzed. The schematic illustration in Fig. 4.13 a (inset) depicts the different types of grain shapes. The aspect ratios of carbonate particles for BLT 12/14 are significantly lower than for BLT 12/08. Accordingly, carbonate particles of BLT 12/14 are more isometric. The results for BLT 12/10 and 12/11 (Fig. 4.13 b) are similar but the difference between the two samples is less pronounced.
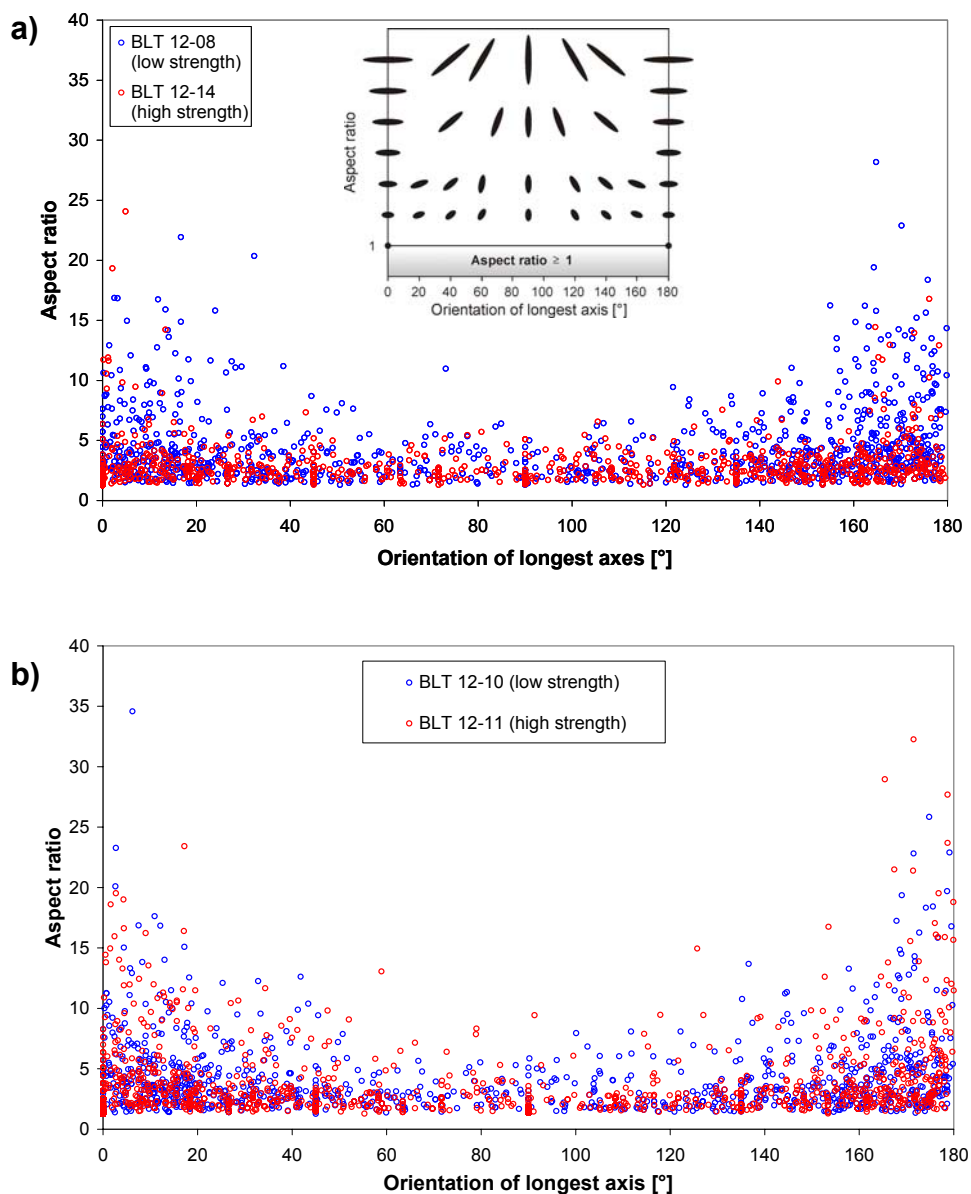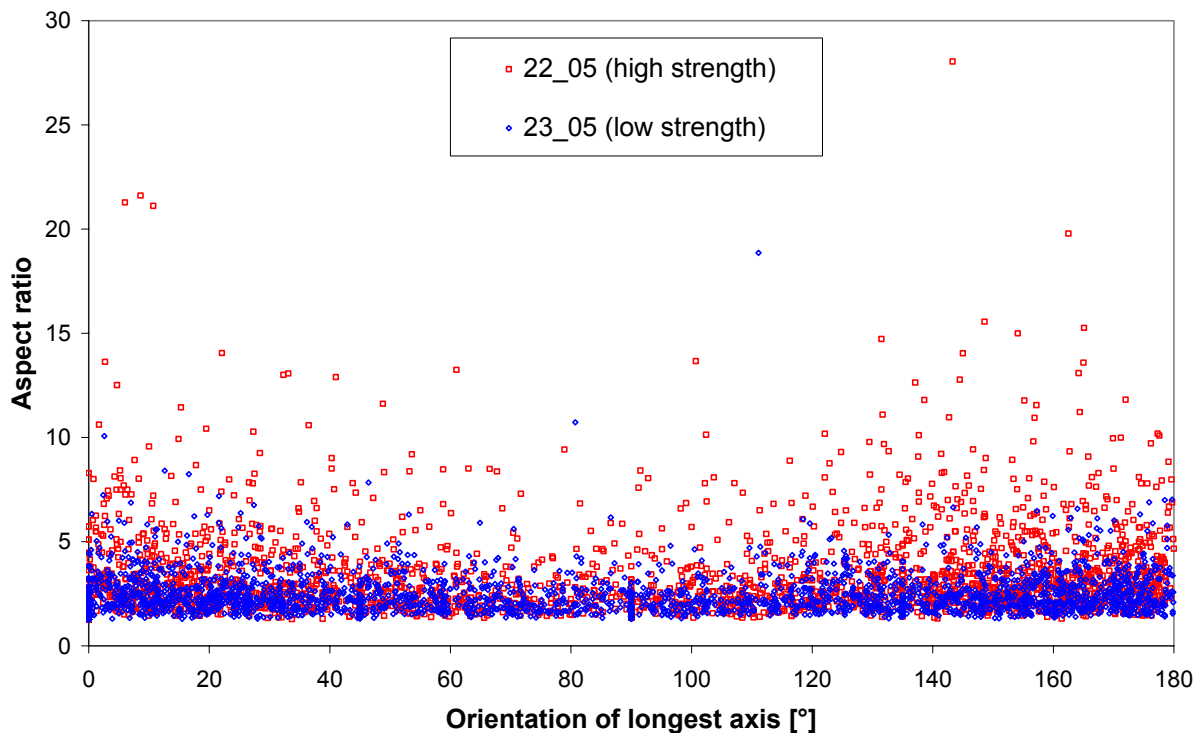

Fig. 4.13: Comparison of the orientation of carbonate particles with respect to the bedding versus aspect ratio (longest axes/shortest axis) **a)** BLT 12/08 (blue: low strength) and BLT 12/14 (red: high strength) **b)** BLT 12/10 (blue: low strength) und BLT 12/11 (red: high strength). 2000 particles analyzed per sample. In Fig. 4.13 a a schematic drawing illustrates the idealized grain shape depending on the location of data points in the diagram with respect to the bedding and the aspect ratio.

The frequency distribution of the angles of the longest axis of the extracted and filtered carbonate grains relative to bedding in steps of 15° is shown in Fig. 4.14. In Fig. 4.14 a the samples BLT 12/08 and BLT 12/14 are compared (images Fig. 4.11). Most of the particles (40 %) are oriented between 0° and 15° with respect to the bedding. Only 20 % of the particles have angles higher than 45°. This is confirmed by the investigation of samples BLT 12/10 and 12/11 (Fig. 4.14 b, images Fig. 4.12).
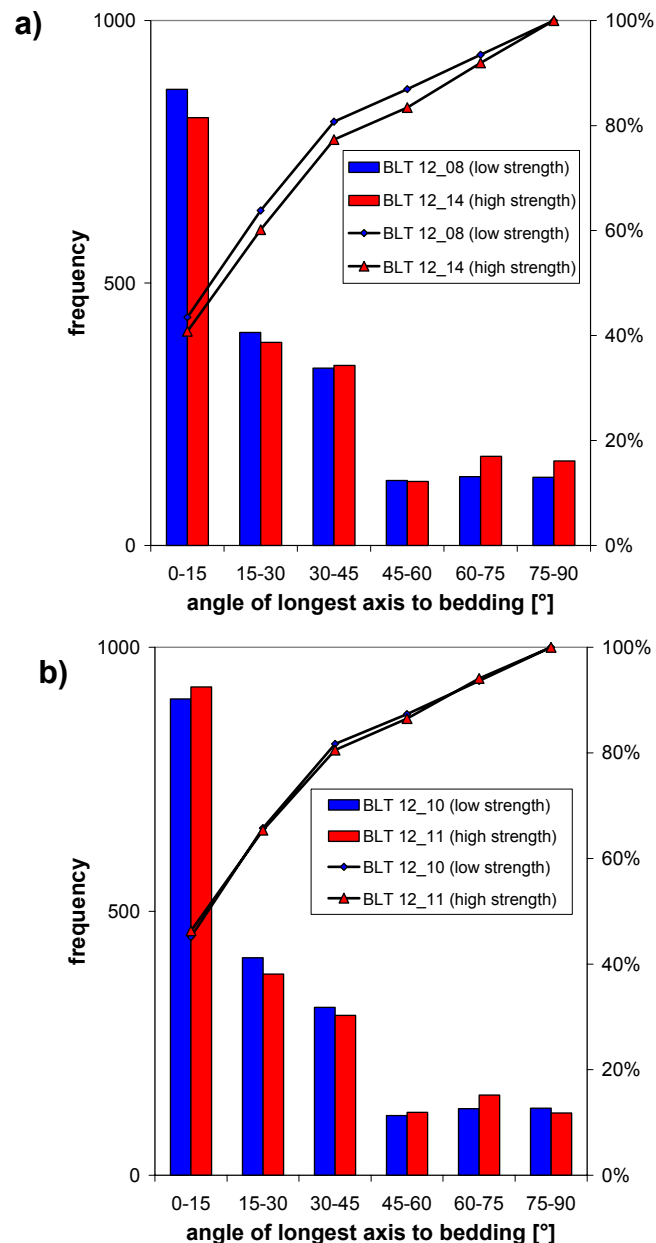
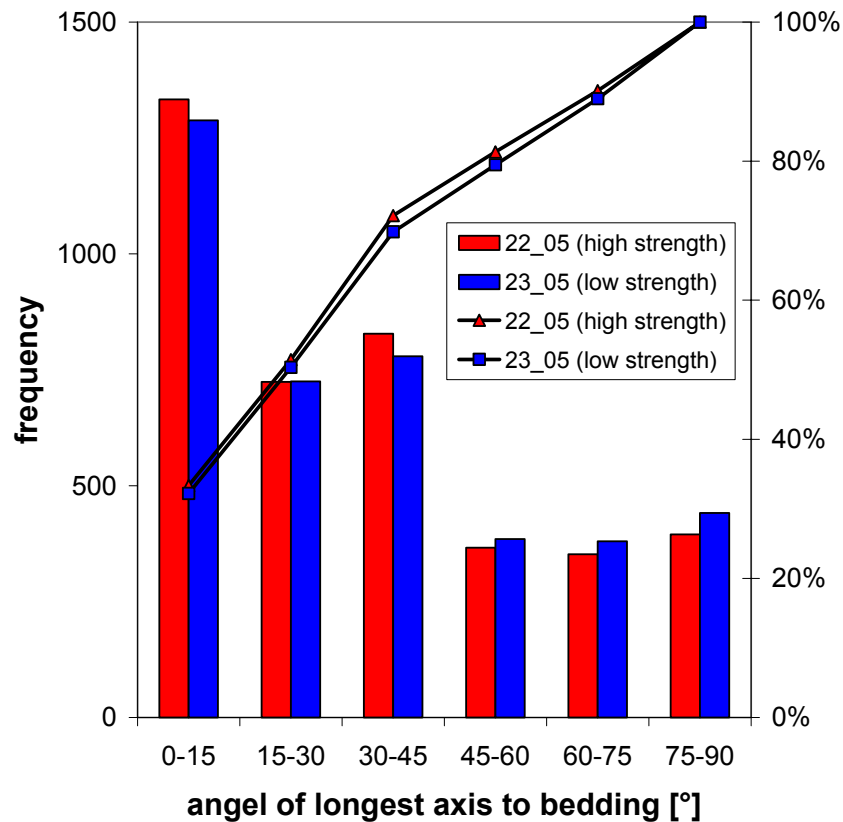**Fig. 4.14:** Comparison of the frequency and cumulative frequency (%) of angle of longest axis relative to bedding of extracted and filtered carbonate grains of Opalinus Clay a) BLT 12/08 and BLT 12/14, b) BLT 12/10 and BLT 12/11. Red: higher failure strength, blue: lower failure strength. 2000 particles analysed per sample.

The aspect ratios of all investigated BLT-samples are depicted in Fig. 4.15. The schematic diagram (upper right corner) in Fig. 4.15 illustrates the idealized shapes of particles depending on the position of a data point with respect to the shortest and longest axis. Particles having axes of equal length (y = x straight line) are isometric (circles). Elongation of particles increases with increasing ratio of longest to shortest axis. Samples with lower failure strength values (BLT 12/07, BLT 12/08, and BLT 12/10) are marked in blue and samples with higher failure strength values (BLT 12/11, BLT 12/13, BLT 12/14, and BLT 12/15) are marked in red. All samples with higher failure strength values are characterised by lower aspect ratios, which indicate more isometric grains, except for sample BLT 12/11. However, a more uniform picture is gained from the carbonate grain size distribution (following discussion).
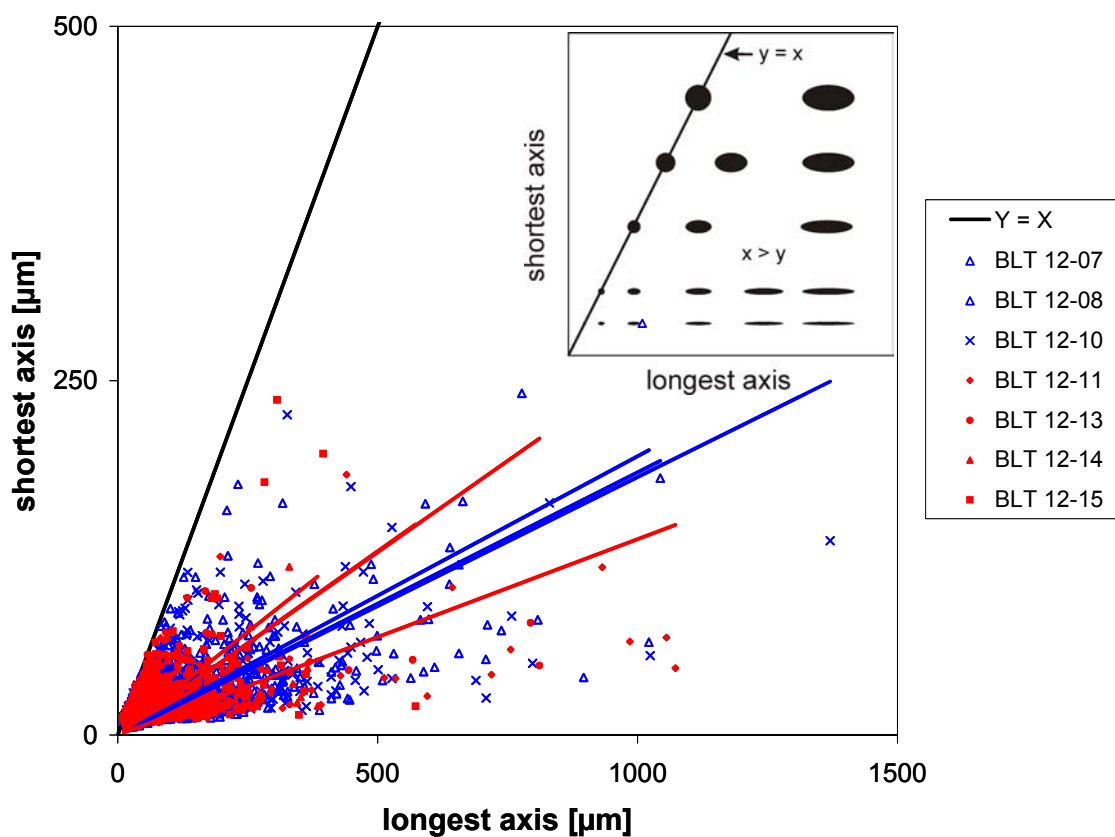
Fig. 4.15: Aspect ratios (longest axis / shortest axis) of carbonate grains of all investigated Opalinus Clay samples of bore hole BLT 12. Red: samples with higher failure strength, blue: samples with lower failure strength. The schematic diagram (inset) illustrates the idealized particle shape depending on the data point position with respect to the shortest and longest axis.

The grain size distributions of carbonate particles of BLT 12/08, BLT 12/14, BLT 12/10, and BLT12/11 are given in Fig. 4.16. Again, 2000 particles were analysed per sample. BLT 12/08 (low failure strength) has a higher content of particles > 63 µm compared to BLT 12/14 (Fig. 4.16 a). Sample BLT 12/14 only has a minor portion of grains coarser than 63 µm. The grain size distributions of carbonate particles of BLT 12/10 and BLT 12/11 are similar (Fig. 4.16 b) compared to BLT 12/08 and BLT 12/14. The content of particles > 63 µm is higher for BLT 12/10 (lower failure strength).
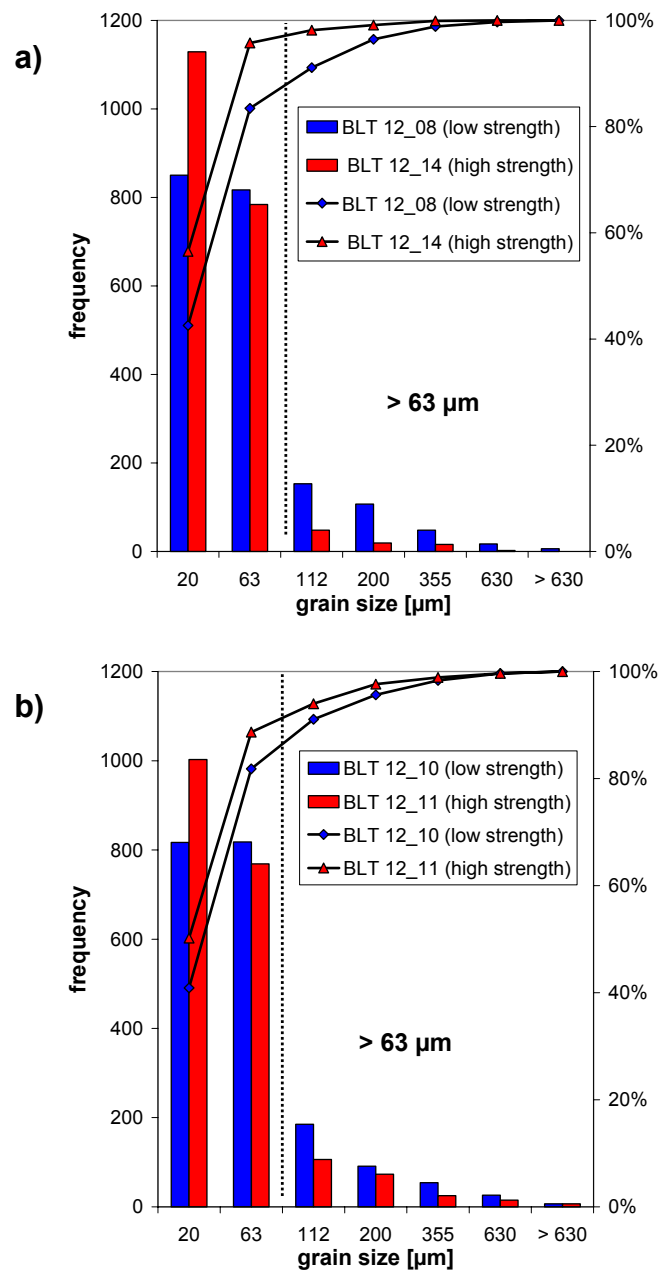
Fig. 4.16: Carbonate grain size distribution of Opalinus Clay: frequency and cumulative frequency (%) of 2000 analysed particles per sample **a)** BLT 12/08 and BLT 12/14 **b)** BLT 12/10 and BLT 12/11. Blue: lower failure strengths, red: higher failure strengths.

The carbonate grain size distribution of all investigated Opalinus Clay samples is illustrated in Fig. 4.17. 2000 particles were analysed per sample (exception: BLT 12/07 only 1599 particles). The failure strength values of samples plotted in red are higher. This indicates that the content of the carbonate grains > 63 µm is particularly important with respect to the mechanical behaviour of the rock.
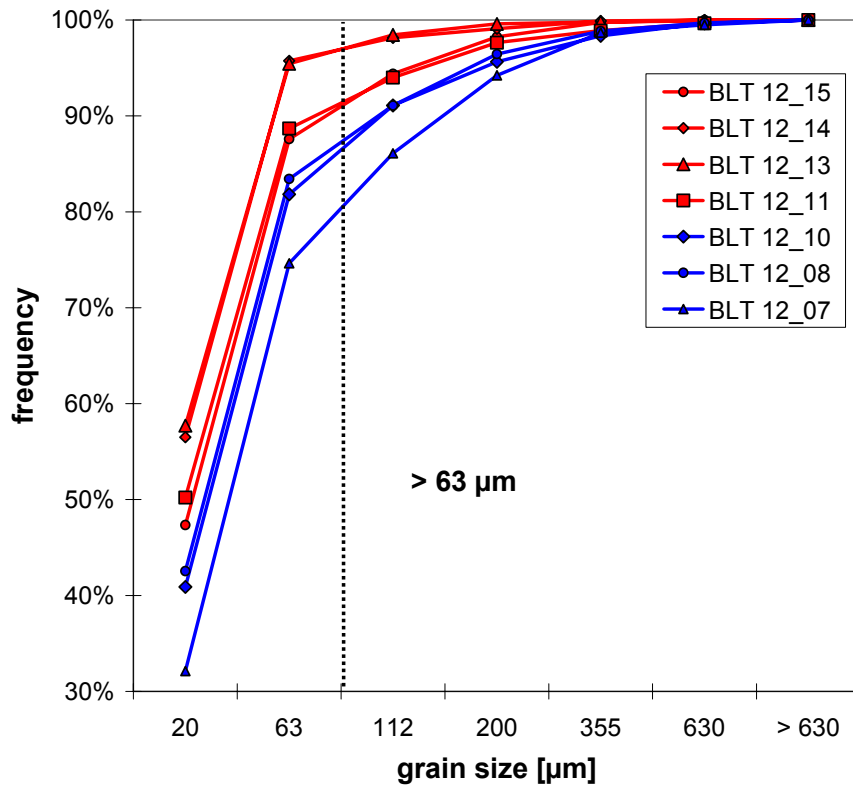
Fig. 4.17: Carbonate grain size distribution of all investigated Opalinus Clay samples of BLT 12 OPA samples of BLT 12 (cumulative frequency). Blue: lower failure strengths, red: higher failure strengths.

Callovo-Oxfordian Clay-stone

Callovo-Oxfordian clay-stones have a clayey matrix containing carbonate particles (light grey, see Fig. 4.18 a). These particles are both shell fragments and idiomorphic calcite crystals. In addition, some quartz grains, partially rounded, could be observed (Fig. 4.18 b), which is not further investigated in the present study. Interestingly, Ca/Mg-carbonates (dolomite) are zoned (Fig. 4.18, Ca-rich areas are brighter). Ca-carbonates have irregular (dendritic) grain boundaries and sometimes a pronounced dovetail connection with the matrix (Fig. 4.18 d). Pyrite occurs both as single idiomorphic crystals and as aggregates (framboides).
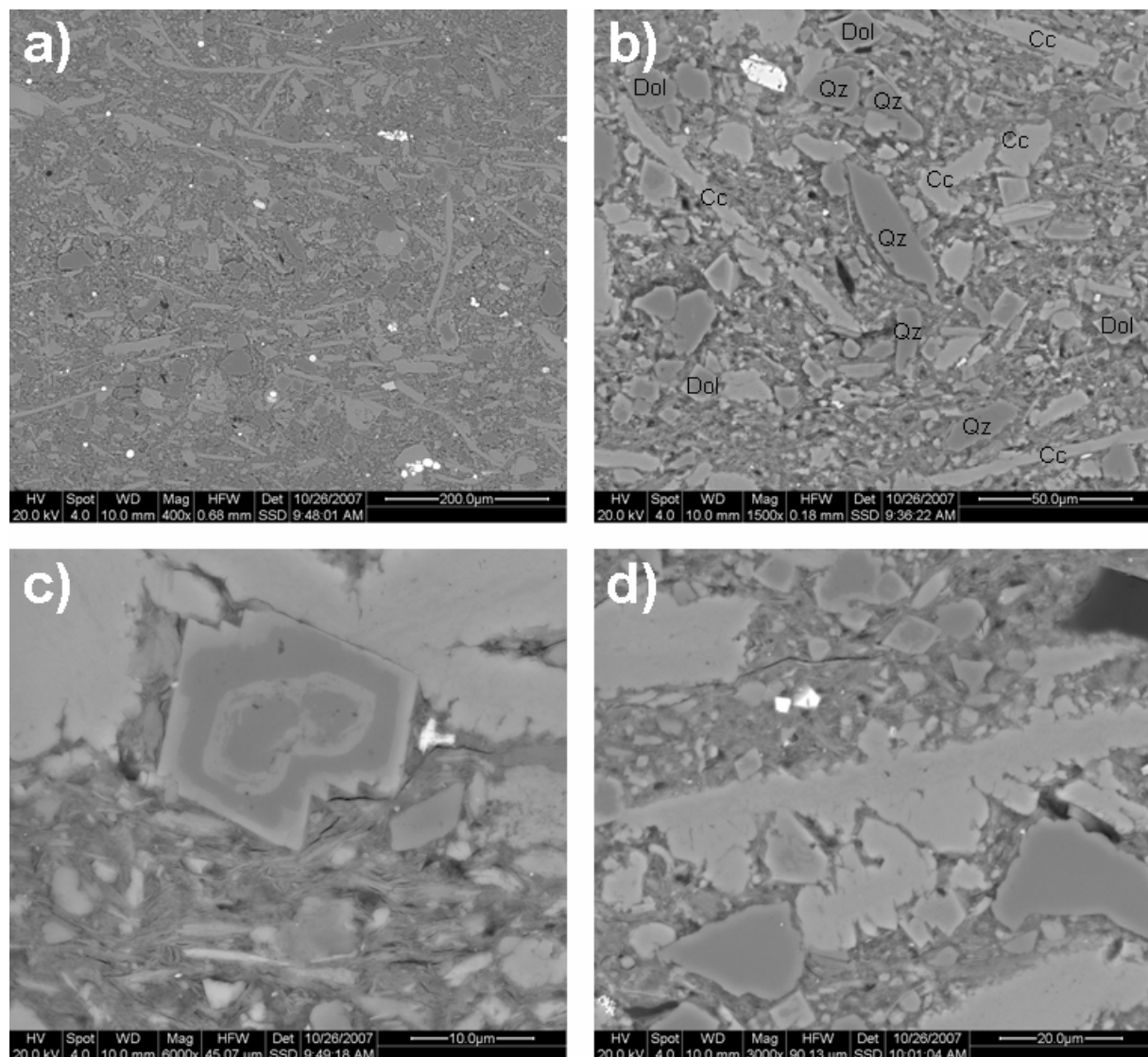
Fig. 4.18: BSE images of Callovo-Oxfordian clay-stone 22_05 **a)** distribution of Ca-carbonate (light grey) in the clayey matrix, **b)** distribution of quartz (Qz), dolomite (Dol), and Calcite (Cc), **c)** zoned crystal of Mg/Ca-carbonate (bright areas Mg-poor, darker areas Mg-rich), and **d)** dovetail connection of Ca-Carbonate with the matrix.

The carbonate microfabric of Callovo-Oxfordian clay-stone 22_05 (carbonate content: 45 wt. %) and 23_05 (carbonate content: 26 wt. %) is compared in Fig. 4.19.
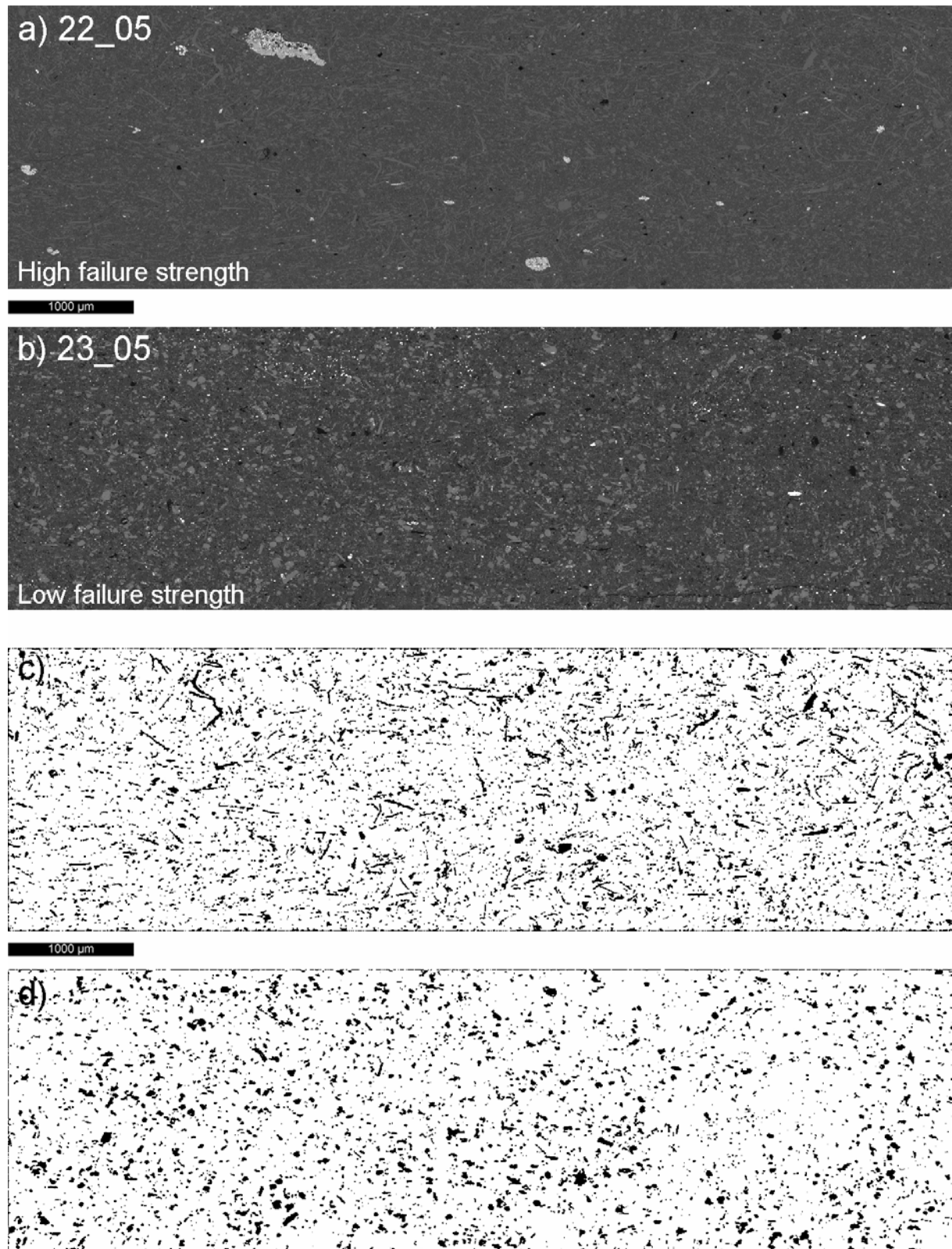
Fig. 4.19: Comparison of the microfabric of Callovo-Oxfordian clay-stone samples **a)** 22_05, BSE-image (high failure strength), **b)** 23_05, BSE-image (low failure strength), **c)** extracted carbonates of 22_05, and **d)** extracted carbonates of 23_05.

In Fig. 4.19 a & b representative BSE-images of samples 22_05 (Fig. 4.19 a) and 23_05 (Fig. 4.19 b) are given. The extracted carbonates are depicted in Fig. 4.19 c & d. Sample 22_05 has a higher failure strength value than sample 23_05. The observed carbonates generally are fine grained and homogeneously distributed in the clayey matrix. Carbonates of sample 22_05 are even finer grained and more elongated. Consequently, the carbonates of sample 23_05 are more isometric.

Fig. 4.20 shows the orientation versus aspect ratio of 4000 analyzed carbonate grains of samples 22_05 (red) and 23_05 (blue). The aspect ratios of sample 22_05 are higher than those of sample 23_05. Accordingly, particles of 22_05 are more elongated and particles of 23_05 are more isometric which is in agreement with the optical observations (Fig. 4.19 a & b).

Fig. 4.20: Comparison of the orientation of carbonate particles with respect to the bedding versus aspect ratio (longest axes/shortest axis) of Callovo-Oxfordian clay-stones 22_05 (red, higher failure strength) and 23_05 (blue, lower failure strength). 4000 particles analysed per sample.

Generally particles are oriented (sub)parallel to bedding. 35 % of the particles are oriented with an angle of 0 to 15 ° to the bedding plane (Fig. 4.21). 30 % of the particles show angles higher than 45 °.

Fig. 4.21: Comparison of the frequency and cumulative frequency (%) of the angle of the longest axis relative to bedding of Callovo-Oxfordian clay-stone 22_05 (red, high failure strength) and 23_05 (blue, low failure strength). 4000 particles analysed per sample.

Differences of the aspect ratios are more evident in Fig. 4.22. Accordingly, more carbonate particles of sample 22_05 are elongated compared to sample 23_05. On average carbonate particles of sample 23_05 are more isometric. Owing to the overall smaller grain sizes of the particles of the Callovo-Oxfordian clay-stone, a larger scale was chosen in order not to loose any carbonate information. For a better comparison with Opalinus Clay the small diagram (upper right corner) is scaled as the Opalinus Clay diagram (Fig. 4.15).

The grain size distribution of 4000 carbonate particles of Callovo-Oxfordian clay-stones does not show significant differences (Fig. 4.23).
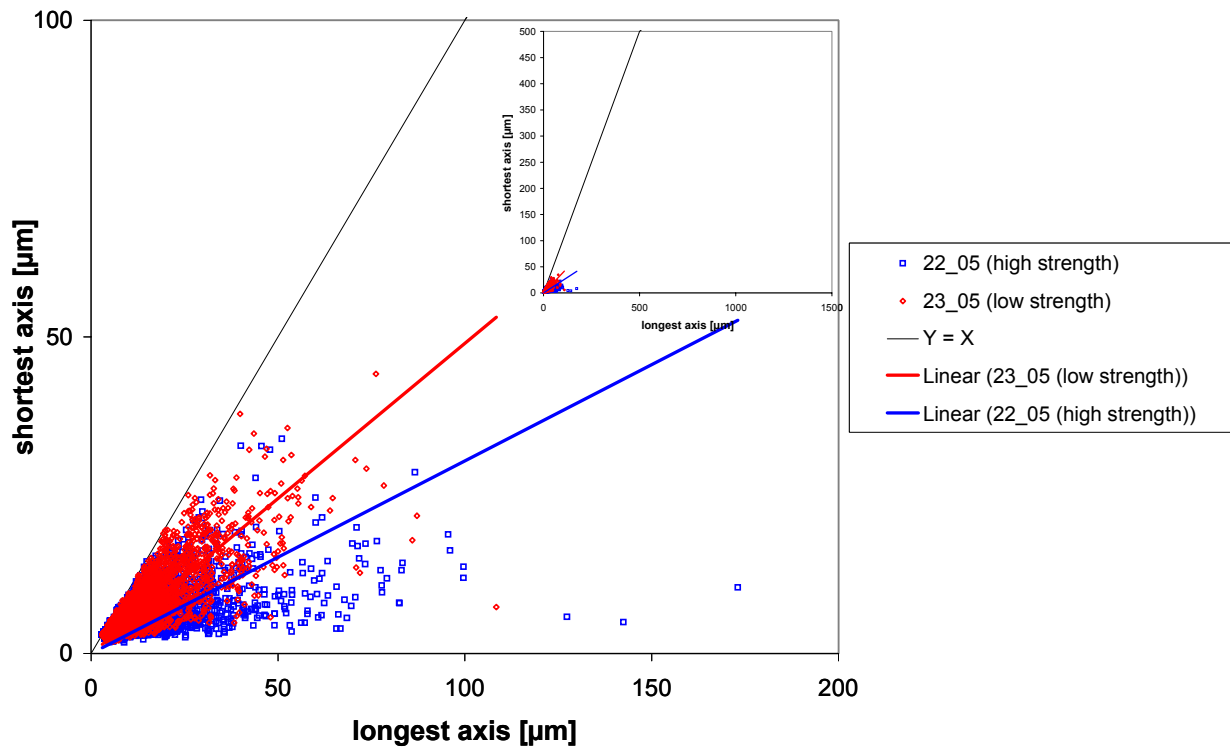
Fig. 4.22: Comparison of aspect ratios (longest axis / shortest axis) of carbonate particles of Callovo-Oxfordian clay-stones 22_05 (red) and 23_05 (blue). Blue: samples with higher failure strength, red: samples with lower failure strength. For better comparison the small diagram (upper right corner) is scaled like the diagram of Opalinus Clay (see Fig. 4.15).
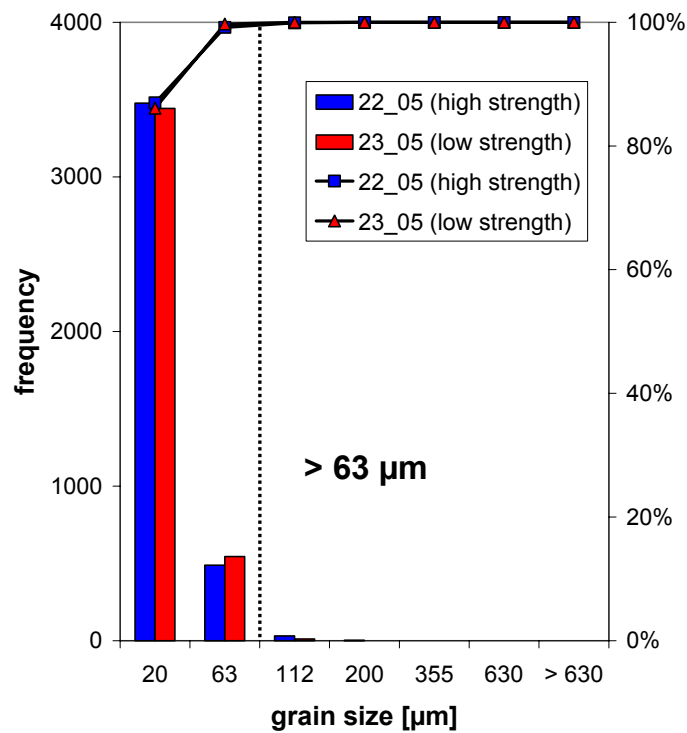
Fig. 4.23: Carbonate grain size distribution of Callovo-Oxfordian clay-stones 22_05 (blue) and 23_05 (red). Frequency and cumulative frequency (%) of 4000 analysed particles per sample. Blue: lower failure strength, red: higher failure strength.

Comparison of Opalinus Clay and Callovo-Oxfordian clay-stone

Opalinus Clay and Callovo-Oxfordian clay-stone behave differently with respect to their mechanical behaviour depending on the carbonate content. Generally, the failure strength of Opalinus Clay decreases with increasing carbonate content while the failure strength of Callovo-Oxfordian clay-stone increases. The difference of the mechanical behaviour can be explained by the microfabric.

Opalinus Clay and Callovo-Oxfordian clay-stone contain carbonates of different shapes and sizes. Fig. 4.24 depicts samples with approximately the same carbonate content: Opalinus Clay BLT 12/10 with 21 wt. % (Fig. 4.24 a & c) and Callovo-Oxfordian clay-stone with 26 wt. % (Fig. 4.24 b & d). Opalinus Clay contains many coarse-grained shell fragments while Callovo-Oxfordian clay-stone containing homogeneously distributed fine grained carbonates. This is confirmed clearly by images of the extracted carbonates (Fig. 4.24 c & d). For image analysis of both samples, 4000 particles each were considered. Obviously, the carbonates are more isometric in case of Callovo-Oxfordian clay-stone which is reflected by lower aspect ratios (Fig. 4.25). Opalinus Clay shows a distinct alignment parallel/sub-parallel to the bedding (Fig. 4.26). The proportion of particles which are oriented with an angle of 0 to 15 ° to the bedding plane is 15 % higher for Opalinus Clay compared to Callovo-Oxfordian clay-stone. Accordingly, the Callovo-Oxfordian clay-stone has a higher proportion of particles oriented with an angle higher than 45°.

The results of the comparison of aspect ratios (longest axis/shortest axis) in Fig. 4.27 confirm the observed differences in shapes of carbonates of the Opalinus Clay and the Callovo-Oxfordian clay-stone. Carbonates of Opalinus Clay are elongated and coarser compared to Callovo-Oxfordian clay-stone.

Fig. 4.28 shows the carbonate grain size distribution. This confirms that carbonate grains of Opalinus Clay are significantly coarser than carbonate grains of the Callovo-Oxfordian clay-stone. For Opalinus Clay, carbonate particles > 63 µm are characteristic. These particles are rare in Callovo-Oxfordian clay-stone. In Callovo-Oxfordian clay-stone 90 % of the carbonate particles are < 20 µm.
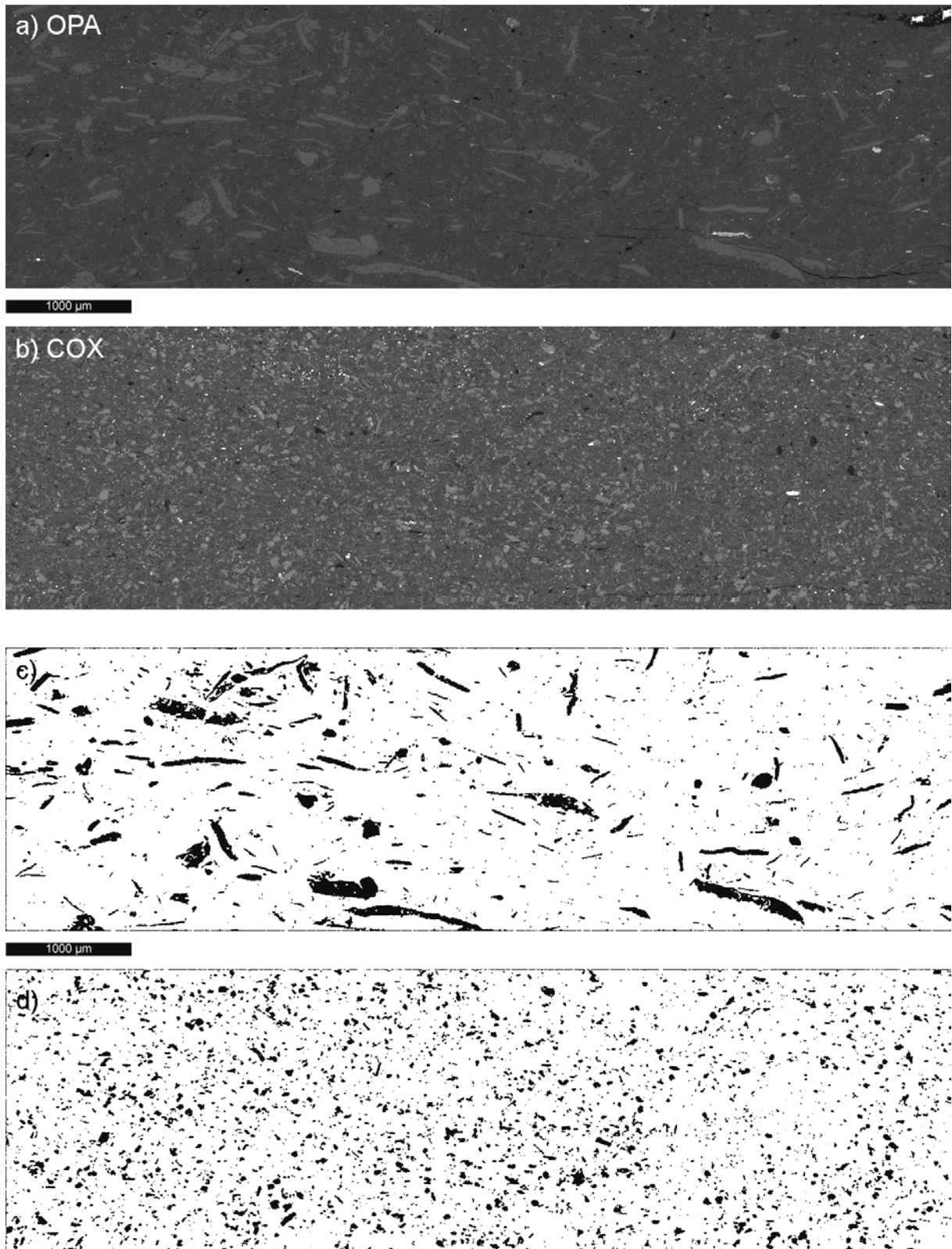
Fig. 4.24: Comparison of carbonate distribution: **a)** Opalinus Clay (OPA) BLT 12/10 (BSE-image), **b)** Callovo-Oxfordian clay-stone (COX) 23_05 (BSE-image), **c)** extracted carbonates of BLT 12/10, and **d)** extracted carbonates 23_05.
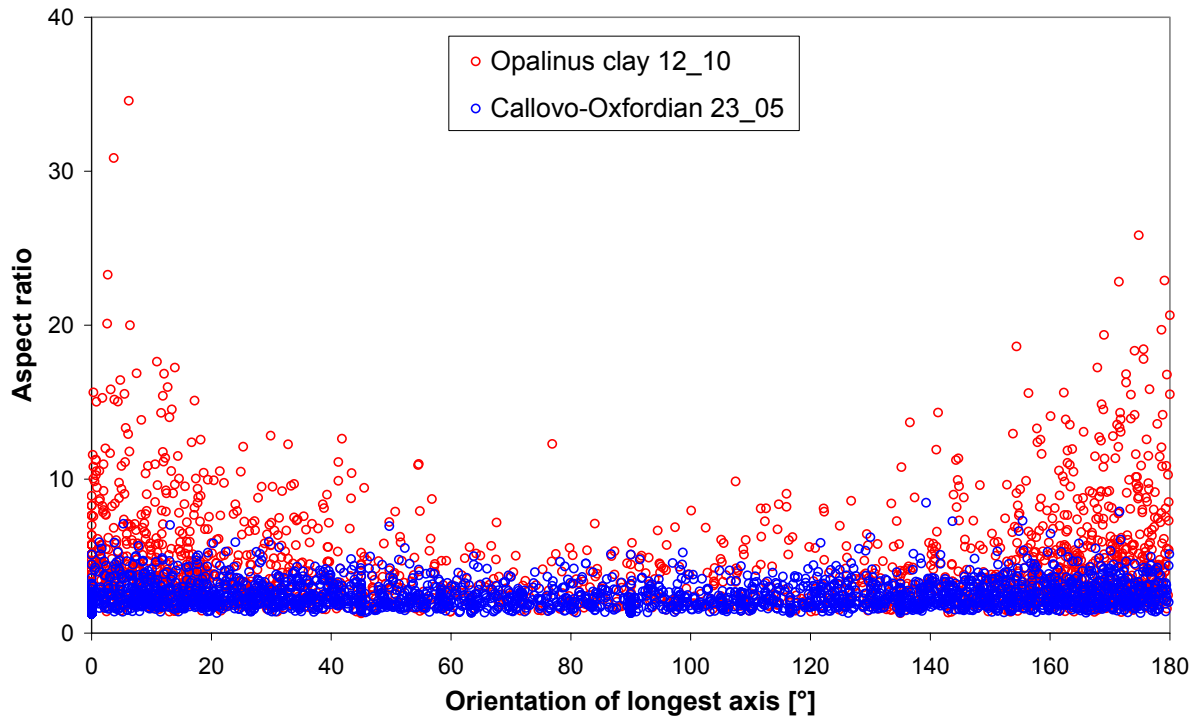
Fig. 4.25: Comparison of the orientation of carbonate particles with respect to the bedding versus aspect ratio (longest axes/shortest axis) of Opalinus Clay (red) and Callovo-Oxfordian clay-stone (blue). 4000 particles analysed per sample.
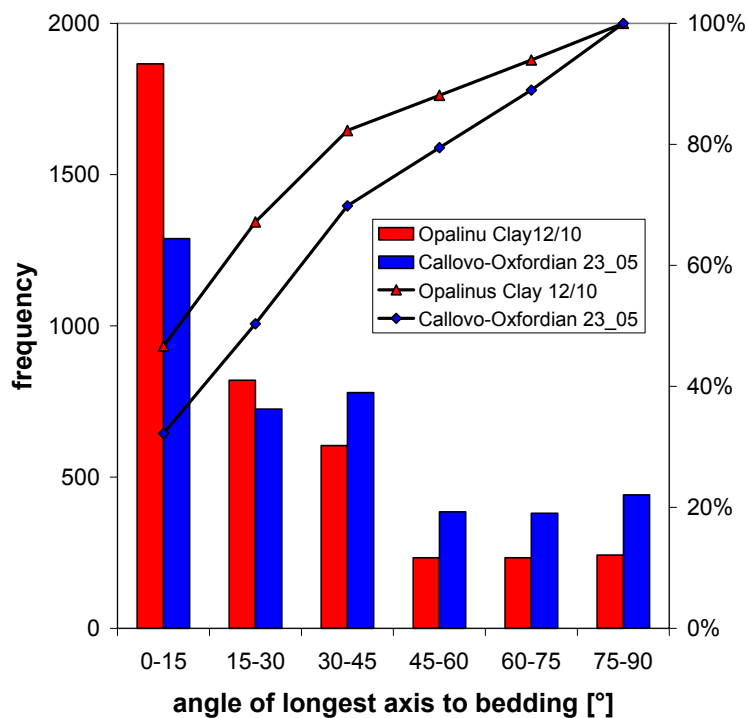
Fig. 4.26: Comparison of the frequency and cumulative frequency (%) of angle of longest axis relative to bedding of Opalinus Clay BLT 12/10 (red) and Callovo-Oxfordian clay-stone 23_05 (blue). 4000 particles analysed per sample.
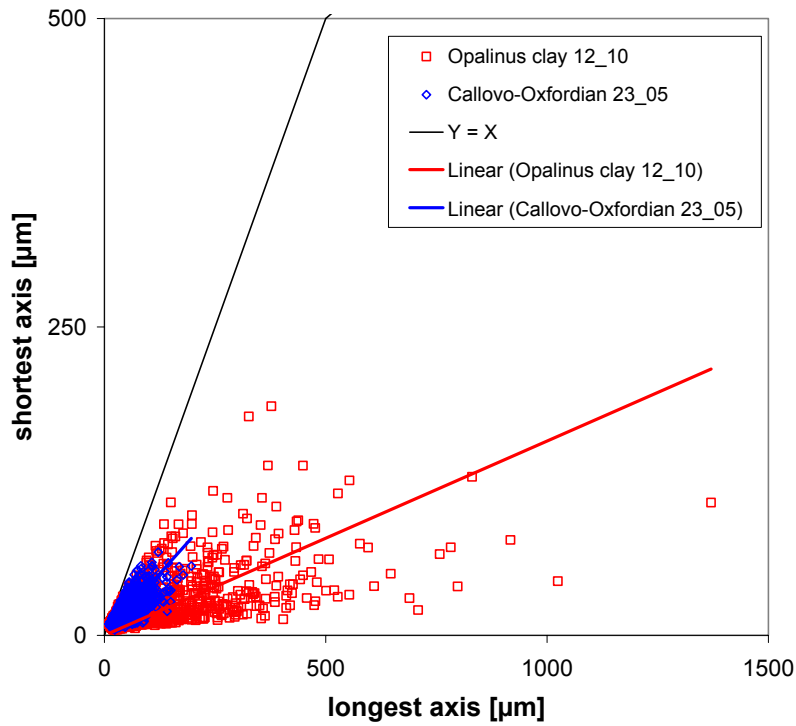
Fig. 4.27: Comparison of aspect ratios (longest axis/shortest axis) of carbonate particles of Opalinus Clay (red) and Callovo-Oxfordian clay-stone (blue). 4000 particles analysed per sample.
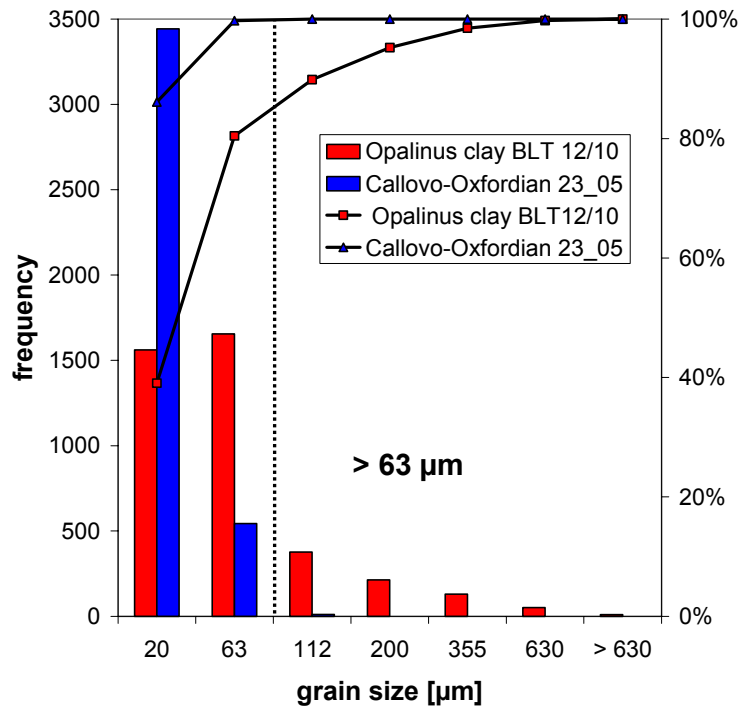
Fig. 4.28: Comparison of grain size distributions of extracted carbonates of Opalinus Clay (red) and Callovo-Oxfordian clay-stone (blue). 4000 particles analysed per sample.

5   Summary and discussion

Clay-stones are currently being investigated as potential host rocks for radioactive waste disposal. The mechanical characteristics of clay-stones are relevant for the stability of the underground facilities and for the characterisation of the behaviour of the whole rock. The results of mechanical tests performed by BGR and other partners of the Mont-Terri project often are difficult to understand because empirical quantitative models (e.g. for modelling of the mechanical behaviour) are missing. To date not all characteristics of clay-stones affecting the mechanical behaviour are fully understood. However, the understanding of the mechanical behaviour of clay-stones is of particular importance for the development of models which are required for performance assessment.

For microfabric analysis, appropriate methods for the optical representation of the fabric are necessary. Therefore, a comparison of different methods was performed e.g. mapping using infrared microscopy and scanning electron microscopy. The results show that BSE images of polished sections provide optimum images for subsequent image analysis aiming at the quantification of parameters of coarse particles like carbonate shell fragments in clay-stones.

The influence of the microfabric and the mineralogical composition on the mechanical behaviour of clay-stones was investigated considering Opalinus Clay and Callovo-Oxfordian clay-stone.

The carbonate content is known to affect the failure strength. Interestingly, for Callovo-Oxfordian clay-stones a positive correlation and for Opalinus Clay a negative correlation was found. This opposite behaviour can be explained by the quantified carbonate fabric data based on image analysis of SEM images.

In case of the Opalinus Clay, cracks are mostly connected to coarse shell fragments. If the shells are close to each other the cracks can be interconnected. Otherwise cracks end in the clayey matrix. This process obviously depends on the carbonate (shell) content, size, shape, and spatial distribution which in turn affect the mechanical strength. The results of carbonate grain size distributions by image analysis prove that samples with lower failure strength contain more coarse particles > 63 µm.

In Callovo-Oxfordian clay-stones, carbonates are supposed to play a completely different role. Most carbonates are fine-grained (90 % < 20 µm). A pronounced dovetail connection with the clayey matrix - which seems to play an important role with respect to the relation of failure strength and carbonate content - was found.

In conclusion the carbonate content as well as the grain size, shape, and spatial distribution influence the mechanical behaviour of calcareous clay-stones. For site investigation of a potential repository for radioactive waste, the mechanical stability of

the underground facilities, e.g. during the construction and deposition phase, and hence the mechanical characteristics of the rock are of particular importance. The differences in carbonate microfabric originate from different sedimentary environments. Hence, fabric characterisation is a valuable tool for site investigation.

6   References

AKEND (2002): Auswahlverfahren für Endlagerstandorte, Empfehlungen des AkEND – Arbeitskreis Auswahlverfahren Endlagerstandorte, 260 S.

ANDRA (1999): Refereniel geologique du site de l'est. A RP ADS 99-005.

APLIN, A.C., FLEET, A.J., MACQUAKER, J.H.S. (1999): Muds and mudstones: physical and fluid-flow properties. In A.C. Aplin, A.J. Fleet, & J.H.S. Macquaker, Eds. Muds and Mudstones: Physical and Fluid-Flow Properties, 158, 1-8. The Geological Society, London.

BAUER-PLAINDOUX, C., TESSIER, D., GHOREYCHI, M. (1998): Propriétés méchaniques des roches argileuses carbonateés: importance de la relation calcite-argile. C. R. Acad. Sci. Paris, Sciences de la Terre et des planètes / Earth and Plantary Sciences, 326, 231-237.

BERGAYA, F. & LAGALY, G. (2006): General introduction: clays, clay minerals, and clay science. In: Bergaya, F., Theng, B.K.G., Lagaly, G. (Eds.) Handbook of clay science. Elsevier, Amsterdam, 1-18.

BERGMANN, J. & KLEEBERG, R. (1998): Rietveld analysis of disordered layer silicates. - Proc. 5th European Conf. on Powder Diffraction (EPDIC 5), Parma, Italy, May 24-28, 1997, Mat. Sci. Forum, 278-281 part 1, 300-305.

BJØRLYKKE, K. (1989): Sedimentology and Petroleum Geology. 363 p. Springer-Verlag, Berlin.

BLATT, H. (1970): Determination of mean sediment thickness in the crust: a sedimentologic method. Geol. Soc. Amer. Bull., 81, 255-262.

BLATT, H., MIDDLETON, G. V., & MURRAY, R. C. (1980): Origin of Sedimentary Rocks. 2. Ed. 782 p. Englewood Cliffs (Prentice-Hall).

BOSSART, P. & THURY, M. (2007): Research in the Mont Terri Rock laboratory: Quo vadis? Physics and Chemistry of the Earth, 32, 19-31.

CHARPENTIER, D., CATHELINEAU, M., MOSSER-RUCK, R., BRUNO, G. (2001): Évolution minéralogique des argilites en zone sous-saturée oxydée: exemple des parois du tunnel de Tournemire (Aveyron, France). C. R. Acad. Sci. Paris, Sciences de la Terre et des planètes / Earth and Plantary Sciences, 332, 601-607.

CHIARELLI, A.S., LEDESERT, B., SIBAI, M., KARAMI, M., HOTEIT, N. (2000): Influence of mineralogy and moisture content on plasticity and induced anisotropic damage of a claystone: application to nuclear waste disposal. Bull. Soc. géol. France, 171(6), 621-627.

CLENNELL, M.B., DEWHURST, D.N., BROWN, K.M., WESTBROOK, G.K. (1999): Permeability anisotropy of consolidated clays. In A.C. Aplin, A.J. Fleet, and J.H.S. Macquaker, Eds. Muds and Mudstones: Physical and Fluid-Flow Properties, 158, 79-96. The Geological Society, London.

COLE, R.D. & PICKARD, M.D. (1975): Primary and secondary sedimentary structures in oil shale and other fine-grained rocks, Green River Formation (Eocene), Utah and Colorado. Utah Geology, 2, 49-67.

DECHER, A. & FRIEDRICH, G. (1991): Bentonite der Cabo de Gata. Die Geowissenschaften, 9(10), 305-316.

DELAY, J., VINSOT, A., KRIEGUER, J.-M., REBOURS, H., ARMAND, G. (2007): Making of the underground scientific experimental programme at the Meuse/Haute-Marne underground research laboratory, North Eastern France. Physics and Chemistry of the Earth, 32, 2-18.

EINSELE, G. (1983): Mechanismus und Tiefgang der Verwitterung bei mesozoischen Ton- und Mergelsteinen. Zeitschrift der deutschen geologischen Gesellschaft, 134, 289-315.

ERNST, TH., FORKEL, W., VON GEHLEN, K. (1959): Vollständiges Nomenklatursystem der Tone. Berichte der Deutschen Keramischen Gesellschaft, 36, 11-18.

ESLINGER, E.V., & PEVEAR, D. (1988): Clay Minerals for Petroleum Geologists and Engineers. 428 p., Society of Economic Paleontologists and Mineralogists, Tulsa.

FABRE, G. & PELLET, F. (2006): Creep and time-dependent damage in argillaceous rocks. Rock Mechanics and Mining Sciences, 43, 950-960.

FOUCHÉ, O., WRIGHT, H., LE CLÉAC'H, J.-M., PELLENARD, P. (2004): Fabric control on strain and rupture of heterogeneous shale samples by using a non-conventional mechanical test. Applied Clay Science, 26, 367-387.

FREIVOGEL, M. & HUGGENBERGER, P. (2003): Modellierung bilanzierter Profile im Gebiet Mont Terri - La Croix (Kanton Jura). In: Heitzmann, P. & Tripet, J. P. (Eds.), Mont Terri Project - Geology, Paleohydrology and Stress Field of the Mont Terri Region. Reports of the Federal Office for Water and Geology (FOWG), 4, 7-44; Bern.

FÜCHTBAUER, H. (1988): Sedimente und Sedimentgesteine. Sediment-Petrologie, II: 4. Ed. 1141 p. Stuttgart (E. Schweizerbart'sche Verlagsbuchhandlung).

GAUCHER, E., ROBELIN, C., MATRAY, J.M., NÉGREL, G., GROS, Y., HEITZ J.F., VINSOT, A., REBOURS, H., CASSAGNABÈRE, A., BOUCHET, A. (2004): ANDRA underground research laboratory: Interpretation of the mineralogical and geochemical data acquired in the Callovian-Oxfordian formation by investigative drilling. Physics and Chemistry of the Earth. 29, 55-77.

GÖBEL, I., ALHEID, H.-J., JOCKWER, N., MAYOR, J. C., GARCIA-SINERIZ, J. L., ALONSO, E., WEBER, H. P., PLÖTZE, M., KLUBERTANZ, G., AMMON, CH. (2007): Heater Experiment (HE): Final Technical Report. – EC Contract-No. FIKW-CT-2001-00132, Bundesanstalt für Geowissenschaften und Rohstoffe (BGR), Hannover.

GU, Y. (2003): Automated Scanning Electron Microscope Based Mineral Liberation Analysis: An Introduction to JKMRC/FEI Mineral Liberation Analyser. Journal of Minerals & Materials Characterization & Engineering, 2(1), 33-41.

GUGGENHEIM, S., ADAMS, J.A., BAIN, D., BERGAYA, F., BRIGATTI, M.F., DRITS, V.A., FORMOSO, M.L.L., GALÁN, E., KOGURE, T., STANJEK,H. (2006): Summery of recommendations of nomenclature committees relevant to clay mineralogy: report of the Association Internationale pour l'Étude des Argiles (AIPEA) nomenclature committee. Clay Minerals, 41(4), 863-877.

HEIM, D. (1990): Tone und Tonminerale: Grundlagen der Sedimentologie und Mineralogie. 157 p., Stuttgart, Enke Verlag.

HEITZMANN, P. & BOSSART, P. (2001): Das Mont-Terri Projekt. Untersuchungen über den Opalinuston im internationalen Felslabor. Bull. angew. Geol., 6(2), 183-197.

HOMM, K. & WEHNER, H. (2003): F + E Endlagerung Organische Geochemie, Organische Petrographie und thermische Versuche an Tonsteinen aus der Bohrung Uthmöden 1/60. 91 p., BGR, Hannover.

HOTH, P., WIRTH, H., REINHOLD, K., BRÄUER, V., KRULL, P., FELDRAPPE, H. (2007): Endlagerung radioaktiver Abfälle in tiefen geologischen Formationen Deutschlands – Untersuchung und Bewertung von Tongesteinesformationen. 118 p., BGR, Berlin/Hannover.

KAUFHOLD, S., DOHRMANN, R., BITZER, C., PLETSCH, T., KLOSA, D. (2004): Post-dismanteling Laboratory Test Results - Mineralogical Investigations (D8a). FIKW-CT-2001-00132: 30 p., Hannover (BGR, R & D final disposal 9Y342101000).

KLOSA, D. (1994): Eine rechnergestützte Methode zur Bestimmung des Gesamtkarbonat-gehaltes in Sedimenten und Böden. Zeitschrift für Angewandte Geologie, 40, 18-21.

LAIRD, D.A. (2006): Influence of layer charge on swelling of smectites. Applied Clay Science, 34, 74-87.

LAMBERT, A. (1997): Ton: kleine Teilchen - große Wirkung. NAGRA informiert, 31, 6-18.

LEWAN, M. D. (1979): Laboratory classification of very fine-grained sedimentary rocks. Geology, 6, 745-748.

MACQUACKER, J.H.S. & ADAMS, A.E. (2003): Maximizing information from fine-grained sedimentary rocks: an inclusive nomenclature for mudstones. J. Sed. Res., 73, 735-744.

MEIER, L.P. & KAHR, G. (1999): Determination of the Cation Exchange Capacity (CEC) of Clay Minerals Using the Complexes of Copper(II) Ion with Triethylenetetramine and Tetraethylenepentamine. Clays and Clay Minerals, 47, 386-388.

MIDTØMME, K., & ROALDSET, E. (1999): Thermal conductivity of sedimentary rocks: uncertainties in measurement and modelling. In A.C. Aplin, A.J. Fleet, and J.H.S. Macquaker (Eds.), Muds and Mudstones: Physical and Fluid-Flow Properties, 45-60. The Geological Society, London.

MONTEIRO, S.N., SILVA, F.A.N., VIEIRA, C.M.F. (2006): Microstructural evaluation of clay ceramic incorporated with petroleum waste. Applied Clay Science, 33, 171-180.

NAGRA (1991): Sedimentstudie - Zwischenbericht 1990 - Zusammenfassende Übersicht der Arbeiten von 1988 bis 1990 und Konzept für das weitere Vorgehen. Technischer Bericht, 91-19, 18 p., Baden, CH (NAGRA).

NAGRA (2002): Projekt Opalinuston - Synthese der geowissenschaftlichen Untersuchungs-ergebnisse - Entsorgungsnachweis für abgebrannte Brennelemente, verglaste hochaktive sowie langlebige mittelaktive Abfälle. Technischer Bericht (NTB), 02-03, 659 p., Wettingen, CH (NAGRA).

NAUMANN, M. & PLISCHKE, I. (2005): Geomechanical Properties of Callovo-Oxfordian Argillites from the Neuse/Haute-Marne Underground Research Laboratory: rapport d'étude; R & D final disposal 9Y321407, BGR, Hannover, 71 p.

NÜESCH, R., (1991): Das mechanische Verhalten von Opalinuston. PhD Thesis, ETH Zürich. 244 p.

O'BRIEN, N.R. & SLATT, R.M. (1990): Argillaceous Rock Atlas. 141 p., Springer, New York.

PETLEY, D. N. (1999): Failure envelopes of mudrocks at high confining pressures. In: Aplin, A. C., Fleet, A. J. & Macquaker, J. H. S. (Eds.), Muds and Mudstones: Physical and Fluid-Flow Properties. Geological Society Special Publication, 158, 61-71, London (The Geological Society).

PICKARD, M.D. (1971): Classification of fine-grained sedimentary rocks. J. Sed. Petrol., 41, 179-795.

PLÖTZE, M., KAHR, G., HERMANNS STENGELE, R. (2003): Alteration of clay minerals - gamma-iradiation effects on physicochemical properties. Applied Clay Science, 23, 175-202.

POTTER, P.E., MAYNARD, J.B., PRYOR, W.A. (1980): Sedimentology of Shale. 306 p., Springer, New York.

PUSCH, R. (1999): Microstructural evolution of buffers. Engineering Geology, 54, 33-41.

PUSCH, R., BÖRGESSON, L., FREDERIKSSON, A., JOHANNESSON, L.-E., HÖKMARK, H., KARNLAND, O., SANDEN, T. (1995): The buffer and backfill handbook. Technical Report 95-45, SKB, Clay Technology AB.

PUSCH, R. & SCHOMBURG, J. (1999): Impact of microstructure on the hydraulic conductivity of undisturbed and artificially prepared smectitic clay. Engineering Geology, 54, 167-172.

RIETVELD, H.M. (1967): Line profiles of neutron powder-diffraction peaks for structure refinement. Acta Crystallographica, 22, 151-152.

SAMMARTINO, S., BOUCHET, A., PRÊT, D., PARNEIX, J.C., TEVISSEN, E. (2003): Spatial distribution of porosity and minerals in clay rocks from the Callovo-Oxfordian formation (Meuse/haute Marne, Eastern France) – implications on ionic species diffusion and rock sorption capability. Applied Clay Science, 23, 157-166.

SCHNIER, H. (2004): Documentation of laboratory triaxial strength tests, FIKW-CT-2001-00132, 17 p., BGR, Hannover.

SCHNIER, H. & STÜHRENBERG, D. (2006): LT Experiment: Strength tests on cylindrical specimens, documentation and evaluation (phase 8 & 9). Technical Note 2004-87, BGR, Hannover.

STOW, D.A.V. & PIPER, D.J.W. (1984): Deep-water fine-grained sediments: history, methodology and terminology. In: Stow, D.A.V. & Piper, D.J.W. (Eds.), Geological Society, London, Special Publications, 15, 3-14; Oxford (Blackwell).

TAUT, T., KLEEBERG, R., BERGMANN, J. (1998): The new Seifert Rietveld program BGMN and its application to quantitative phase analysis. Mater. Struct., 5-1, 57-64.

TOURTELOT, H.A. (1960): Origin and use of the word "shale". Am. Jour. Sci., 258, 335-343.

THURY, M. (1997): Das Felslabor Mont Terri. NAGRA informiert, 31, 33-44.

THURY, M., & BOSSART, P. (1999): The Mont Terri rock laboratory, a new international research project in a Mesozoic shale formation, in Switzerland. Engineering Geology, 52, 347-359.

UFER, K., ROTH, G., KLEEBERG, R., STANJEK, H., DOHRMANN, R., BERGMANN, J. (2004): Description of X-ray powder pattern of turbostratically disordered structures with a Rietveld compatible approach. Zeitschrift für Kristallographie, 219, 519-527.

VAN LOON, L. R. (2002): Anisotropic diffusion in layered argillaceous rocks: A case study with Opalinus Clay. Workshop on clay microstructure and its importance to soil behaviour, Lund, Sweden, 197-213.

WIGNALL, P.B. (1994): Black Shales. Oxford Monographs on Geology and Geophysics, 30, 144 p., Oxford University Press, Oxford, USA.

YONG, R.N. (2003): Influence of microstructural features on water ion diffusion and transport in clay soils. Applied Clay Science, 23, 3-13.

YONG, R.N. & MULLIGAN, C.N. (2003): The impact of clay microstructural features on the natural attenuation of contaminants. Applied Clay Science, 23, 179-186.

7   List of figures

8   List of tables

9   List of abbreviations

BSE	Backscattered electrons
CEC	Cation exchange capacity
EDS	Energy Dispersive X-Ray Spectroscopy
ESEM	Environmental scanning electron microscope
ICP-OES	Inductive coupled plasma – optical emission spectroscopy
LOI	Loss on ignition
RT	Roomtemperature
SEM	Scanning electron microscope
TC	Total carbon
TOC	Total organic carbon
TS	Total sulphur
URL	Underground rock laboratory
XRD	X-ray diffraction
XRF	X-ray fluorescence
Cc	Calcite
Dol	Dolomite
Qz	Quartz